HHS Public Access

Author manuscript

*Dev Cell*. Author manuscript; available in PMC 2023 April 11.

Published in final edited form as:

*Dev Cell*. 2022 April 11; 57(7): 883–900.e10. doi:10.1016/j.devcel.2022.03.005.

# A translation control module coordinates germline stem cell differentiation with ribosome biogenesis during *Drosophila* oogenesis

**Elliot T. Martin**[1,*], **Patrick Blatt**[1,*], **Elaine Nguyen**[2], **Roni Lahr**[2], **Sangeetha Selvam**[1], **Hyun Ah M. Yoon**[1,3], **Tyler Pocchiari**[1,4], **Shamsi Emtenani**[5], **Daria E. Siekhaus**[5], **Andrea Berman**[2], **Gabriele Fuchs**[1,†], **Prashanth Rangan**[1,#,6,†,7]

[1]Department of Biological Sciences/RNA Institute, University at Albany SUNY, Albany, NY 12202, USA

[2]Department of Biological Sciences, University of Pittsburgh, Pittsburgh, PA 15260, USA

[3]Albany Medical College, Albany, NY 12208, USA

[4]SUNY Upstate Medical University, Syracuse, NY 13210-2375, USA

[5]Institute of Science and Technology Austria, 3400 Klosterneuburg, Austria

[6]Department of Cell, Developmental and Regenerative Medicine, Black Family Stem Cell Institute, Icahn School of Medicine at Mount Sinai, One Gustave L. Levy Place Box 1020 New York, NY 10029-6574, USA

[7]Lead contact

## Summary:

Ribosomal defects perturb stem cell differentiation, causing ribosomopathies. How ribosome levels control stem cell differentiation is not fully known. Here we discovered that three DExD/H-box proteins govern ribosome biogenesis (RiBi) and *Drosophila* oogenesis. Loss of these DExD/H-box proteins, which we named Aramis, Athos and Porthos, aberrantly stabilized p53, arrested the cell cycle, and stalled GSC differentiation. Aramis controls cell cycle progression by regulating translation of mRNAs containing a Terminal Oligo Pyrimidine (TOP) motif in their 5'-UTRs. We find TOP motifs confer sensitivity to ribosome levels mediated by La-related protein (Larp). One such TOP-containing mRNA codes for Novel Nucleolar protein 1 (Non1), a conserved p53 destabilizing protein. Upon a sufficient ribosome concentration, Non1 is expressed and promotes GSC cell cycle progression via p53 degradation. Thus, a previously unappreciated

[†]Co-corresponding authors: gfuchs@albany.edu, prangan@albany.edu.
[#]Current Address
[*]These authors contributed equally to this work

Author Contributions

Conceptualization, E.T.M., P.B., G.F., and P.R.; Methodology, E.T.M., P.B., G.F., and P.R.; Investigation, E.T.M., P.B., E.N., R.L., S.S., H.Y., T.P., and S.E.; Writing, E.T.M., P.B., D.E.S, A.B., G.F., and P.R.; Funding Acquisition, G.F. and P.R.; Visualization, E.T.M., E.N.; Supervision, G.F. and P.R.

TOP-motif in *Drosophila* responds to reduced RiBi to co-regulate the translation of ribosomal proteins and a p53 repressor, coupling RiBi to GSC differentiation.

## Graphical Abstract

Stem cell differentiation is sensitive to ribosome biogenesis but how ribosome biogenesis is coupled to stem cell differentiation is not fully elucidated. Martin et al. describe a pathway that couples production of ribosomal proteins and cell cycle progression to allow for female *Drosophila* GSCs to successfully differentiate.

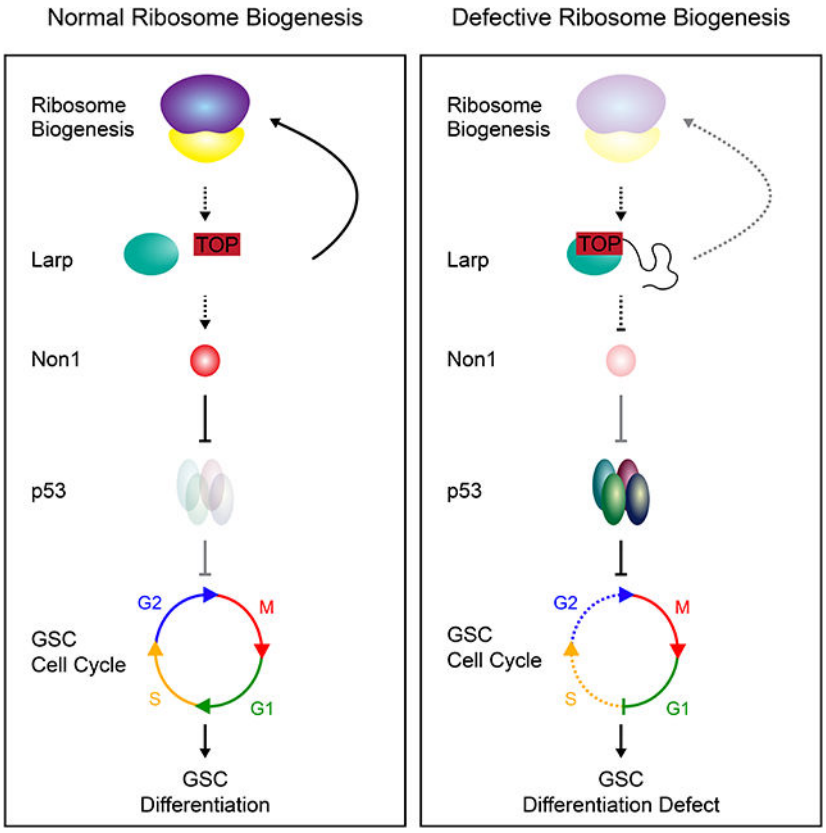


## Introduction

All life depends on the ability of ribosomes to translate mRNAs into proteins. Despite this universal requirement, perturbations in ribosome biogenesis (RiBi) affects some cell types more than others. Stem cells, a cell type that underlies the generation and expansion of tissues, have an increased ribosomal requirement (Gabut et al., 2020; Sanchez et al., 2016; Woolnough et al., 2016; Zhang et al., 2014). Ribosome production is dynamically regulated to maintain higher amounts in stem cells. Reduction of ribosome levels in several stem cell systems can cause differentiation defects (Corsini et al., 2018; Khajuria et al., 2018; Zhang et al., 2014). In *Drosophila,* perturbations that reduce ribosome levels in the GSCs result in differentiation defects causing infertility (Sanchez et al., 2016). Similarly, humans with impaired RiBi are afflicted with clinically distinct diseases known as ribosomopathies, such as Diamond-Blackfan anemia, that often result from loss of proper differentiation of

tissue-specific progenitor cells (Higa-Nakamine et al., 2012; Lipton et al., 1986; Mills and Green, 2017). However, the mechanisms by which RiBi is coupled to proper stem cell differentiation remain incompletely understood.

RiBi requires the transcription of ribosomal RNAs (rRNAs) and of mRNAs encoding ribosomal proteins (RPs) (de la Cruz et al., 2015; Granneman et al., 2006; Tafforeau et al., 2013). Hundreds of factors including DExD/H-box proteins transiently associate with maturing rRNAs to facilitate rRNA processing, modification, and folding (Granneman et al., 2011; Sloan et al., 2017; Tafforeau et al., 2013; Watkins and Bohnsack, 2012). RPs are imported into the nucleus, where they assemble with rRNAs in the nucleolus to form precursors to the 40S and 60S ribosomal subunits, which are then exported to the cytoplasm (de la Cruz et al., 2015; Koš and Tollervey, 2010; Nerurkar et al., 2015).

In mammals, mRNAs that encode the RPs contain a Terminal Oligo Pyrimidine (TOP) motif within their 5' untranslated region (UTR), which regulates their translation in response to nutrient levels (Fonseca et al., 2015; Hong et al., 2017). Under growth-limiting conditions, La related protein 1 (Larp1) binds to the TOP sequences and to mRNA caps to inhibit translation of RPs (Fonseca et al., 2015; Jia et al., 2021; Lahr et al., 2017; Philippe et al., 2018). When growth conditions are suitable, Larp1 is phosphorylated by the mammalian Target of rapamycin complex 1 (mTORC1), and does not efficiently bind the TOP sequence, allowing for translation of RPs. Whether TOP motifs exist in *Drosophila* to coordinate RP synthesis is unclear. The *Drosophila* ortholog of Larp1, La related protein (Larp) is required for proper cytokinesis and meiosis in *Drosophila* testis as well as for female fertility, but its targets remain undetermined (Blagden et al., 2009; Ichihara et al., 2007).

Germline depletion of RiBi factors results in a stereotypical GSC differentiation defect during *Drosophila* oogenesis (Sanchez et al., 2016). Female *Drosophila* maintain 2–3 GSCs in the germarium (Figure 1A) (Xie and Spradling, 2000, 1998). Asymmetric cell division of GSCs produces a self-renewing daughter GSC and a differentiating daughter, called the cystoblast (CB) (Figure 1A) (Chen and McKearin, 2003; McKearin and Ohlstein, 1995). This asymmetric division is unusual: following mitosis, the abscission of the GSC and CB is not completed until the following G2 phase (Figure 1A') (De Cuevas and Spradling, 1998; Hsu et al., 2008). The GSC is marked by a round structure called the spectrosome, which elongates and eventually bridges the GSC and CB, similar to the fusomes that connect differentiated cysts (Figure 1A–A'). During abscission the extended spectrosome structure is severed and a round spectrosome is established in the GSC and the CB (Figure 1A') (De Cuevas and Spradling, 1998; Hsu et al., 2008). RiBi defects result in failed GSC-CB abscission, causing cells to accumulate as interconnected cysts called "stem-cysts" that are marked by a fusome-like structure (Figure 1A') (Mathieu et al., 2013; Sanchez et al., 2016). In contrast with differentiated cysts (McKearin and Ohlstein, 1995; Ohlstein and McKearin, 1997), these stem-cysts do not express the differentiation factor Bag of Marbles (Bam), do not differentiate, and typically die, resulting in sterility (Figure 1A') (Sanchez et al., 2016). How proper RiBi promotes GSC abscission and differentiation is not known.

## Results

### Three conserved DExD/H-box proteins are required in the germline for GSC differentiation

In a screen to identify RNA helicases in the germline that are required for female fertility in *Drosophila*, we identified three uncharacterized genes, *CG5589*, *CG4901,* and *CG9253* (Figure 1B–C) (Supplemental Table 1) (Blatt et al., 2021). We named these candidate genes *aramis* (*ais*), *athos* (*ath*), and *porthos* (*pths*), respectively, after Alexandre Dumas' three musketeers. We evaluated the efficiency of germline knockdown (GKD) mediated by RNAi using the germline-driver *nanosGAL4* (*nosGAL4*) in ovaries using qPCR and found that *ais*, *ath*, and *pths* were significantly downregulated relative to control (Figure S1A). Using available GFP::3XFLAG tagged versions of *ais* and *ath* under endogenous control, we found that GKD of each of these genes resulted in reduced Ais and Ath (Figure S1B–D). To further investigate how these genes promote fertility, we performed GKD of *ais*, *ath*, and *pths* and stained for germline and spectrosomes/fusomes using Vasa and 1B1 antibodies, respectively. In contrast to controls, *ais*, *ath*, and *pths* GKD ovaries lacked spectrosome-containing cells, and instead displayed cells with fusome-like structures proximal to the self-renewal niche (Figure 1D–H; Figure S1E–E"'). The cells in this cyst-like structure contained ring canals, a marker of cytoplasmic bridges, suggesting that they are interconnected (Figure S1F–F"') (Zhang et al., 2014). In addition to forming cysts in an aberrant location, the *ais*, *ath*, and *pths* GKD ovaries failed to form egg chambers (Figure S1G–G"').

Aberrant cyst formation proximal to the niche could reflect stem-cysts with GSCs that divide to give rise to CBs but fail to undergo cytokinesis or differentiated cysts that do not differentiate into egg chambers. To discern between these possibilities, we examined the expression of a GSC marker, phosphorylated Mothers against decapentaplegic (pMad). We observed pMad expression in the cells closest to the niche, but not elsewhere in the germline cysts of *ais*, *ath*, and *pths* GKD flies (Figure S1H–H"') (Kai and Spradling, 2003). Additionally, none of the cells connected to the GSCs in *ais*, *ath*, and *pths* GKD flies expressed the differentiation reporter Bam::GFP (Figure 1D–G") (McKearin and Ohlstein, 1995). Thus, *ais*, *ath*, or *pths* GKD results in the formation of stem-cysts, however with variable severity. Overall, we infer that Ais, Ath, and Pths are required for proper GSC cytokinesis to produce a CB.

### Ais, Athos, and Porthos are required for RiBi

Ais, Ath, and Pths are conserved from yeast to humans (Figure 1B). The orthologs of Ais, Ath, and Pths are Rok1, Dhr2, and Rrp3 in yeast and DExD-Box Protein 52 (DDX52), DEAH-Box Protein 33 (DHX33), and DEAD-Box Protein 47 (DDX47) in humans, respectively (Figure 1B) (Hu et al., 2011). Both the yeast and human orthologs have been implicated in rRNA biogenesis (O 'day et al., 1996; Sekiguchi et al., 2006; Tafforeau et al., 2013; Venema et al., 1997; Vincent et al., 2017; Zhang et al., 2011). In addition, the GSC-cytokinesis defect that we observed in *ais*, *ath*, and *pths* GKD is a hallmark of reduced RiBi (Sanchez et al., 2016). Based on these observations, we hypothesized that Ais, Ath, and Pths could regulate RiBi.

Many factors involved in Ribi localize to the nucleolus and interact with rRNA (Grandori et al., 2005; Henras et al., 2008; Karpen et al., 1988). To detect the subcellular localization of Ais and Ath, we used available Ais::GFP::3XFLAG or Ath::GFP::3XFLAG fusion proteins under endogenous control. For Pths, we expressed a Pths::3XFLAG::3XHA fusion under the control of the UASt promoter in the germline using a previously described approach (DeLuca and Spradling, 2018). We found that in the germline, Ais, Ath and Pths colocalized with Fibrillarin, a nucleolar marker (Figure 2A–C”’) (Ochs et al., 1985). Ais was also in the cytoplasm of the germline and somatic cells of the gonad. To determine if Ais, Ath, and Pths directly interact with rRNA, we performed immunoprecipitation (IP) followed by RNAseq. We found that pre-rRNA immunopurified with Ais, Ath, and Pths (Figure 2D–D”, Figure S2A–A”). Thus, Ais, Ath, and Pths are present in the nucleolus and interact with pre-rRNA, suggesting that they might regulate Ribi.

Nucleolar hypotrophy is associated with reduced RiBi (Freed et al., 2012; Panov et al., 2021). If Ais, Ath, and Pths promote RiBi, then their loss would be expected to cause nucleolar stress and a reduction in mature ribosomes. Staining for Fibrillarin, we found hypotrophy of the nucleolus in *ais, ath,* and *pths* GKD flies compared to control (Figure S2B–C’). We used polysome profiling to evaluate the ribosomal subunit ratio and polysome levels in Schneider 2 (S2) cells depleted of *ais*, *ath*, or *pths*. We found that upon the depletion of all three genes, the heights of the polysome peaks were reduced (Figure 2E–E”). Depletion of *ais* and *pths* diminished the height of the 40S subunit peak compared to the 60S subunit peak, characteristic of 40S Ribi defect (Figure 2E, E”, Figure S2D) whereas *ath* depletion diminished the height of the 60S subunit peak compared to the 40S peaks, characteristic of a 60S RiBi defect (Figure 2E’, Figure S2D’) (Cheng et al., 2019). Stem-cyst that arises from depletion of RiBi genes in the germline genetically interact with Shrub (shrb) a member of the Escrt-III complex (Sanchez et al., 2016). To further determine if *ais*, *ath*, and *pths* regulate RiBi, we performed trans-heterozygous crosses between *ais* and *pths* and *shrb*. For *ath*, we used a deficiency line as no mutant was available. We found presence of stem-cysts in *shrb* heterozygotes mutants, as previously observed (Matias et al., 2015; Sanchez et al., 2016), as well as in *ais*, *ath* and *pths* heterozygous mutants (Figure S2E–L). Trans-heterozygous germaria of a *shrb* mutant with mutations in genes of interest resulted in higher levels of stem-cysts than in their respective heterozygous backgrounds, consistent with their role in RiBi (Figure S2E–L). Our findings, taken with the known function of yeast and mammalian homologs, indicate that *ais*, *ath*, and *pths* promote RiBi.

## Ais promotes cell cycle progression via p53 repression

Our data indicated that Ais, Ath and Pths promote RiBi, which is required for GSC abscission (Sanchez et al., 2016). Yet the connections between RiBi and GSC abscission are poorly understood. To explore this, we further examined the *ais* GKD, as its defect was highly penetrant but maintained sufficient germline for analysis (Figure 1E, H). First, we compared the mRNA profiles of *ais* GKD ovaries to *bam* GKD to determine if genes that are known to be involved in GSC abscission were altered. We used germline *bam* GKD as a control because it leads to the accumulation of CBs with no abscission defects (Flora et al., 2018a; McKearin and Ohlstein, 1995), whereas loss of *ais* resulted in accumulation of CBs that do not abscise from the GSCs.

We performed RNAseq and found that 607 RNAs were downregulated and 673 RNAs were upregulated in *ais* GKD versus *bam* GKD ($\log_2$(foldchange)>|1.5|, False Discovery Rate (FDR) < 0.05) (Figure S3A, Supplemental Table 2). Gene Ontology (GO) analysis on differentially expressed genes (Thomas et al., 2003) revealed that downregulated genes upon *ais* GKD were enriched for cell cycle, whereas the upregulated genes were enriched for stress response (Figure 3A, Figure S3B). The downregulated genes included *Cyclin A*, which is required for cell cycle progression, *Cyclin B* (*CycB*) and *aurora B*, which are required for both cell cycle progression and cytokinesis; in contrast *Actin 5C* was unaffected (Figure 3B–C, Figure S3C–C') (Mathieu et al., 2013; Matias et al., 2015). CycB protein was also reduced in the ovaries of *ais* GKD flies compared to *bam* GKD (Figure 3D–F). Double *ais and bam* GKD also result in the same phenotype as *ais* GKD alone (Figure S3D–E'). RNAseq on *ais; bam* double GKD revealed that downregulated genes were also enriched for the GO-term category of cell cycle, consistent with *ais* GKD alone compared to *bam* GKD (Figure 3A, Supplemental Table 3). Similarly, the GO-terms we identified for upregulated genes from the double-depletion are also enriched upon *ais* single depletion (Figure S3B, Supplemental Table 3). Crucially, all the genes we refer to in the manuscript such as *CycB*, *AurB,* and *CycA* are also targets in *bam*; *ais* double GKD. (Figure 3B–C, Figure S3C–C', Supplemental Table 3). These results suggest that *ais* is required for the proper levels of key regulators of GSC abscission.

CycB is expressed during G2 phase to promote GSC abscission (Mathieu et al., 2013). To test if *ais* GKD leads to GSC abscission defects due to diminished expression of CycB, we expressed a functional CycB::GFP fusion protein in the germline under the control of a UAS/GAL4 system (Figure S3F–G) (Mathieu et al., 2013). Unexpectedly, the CycB::GFP fusion protein was not expressed in the *ais* GKD germline, unlike the wild type (WT) germline (Figure S3F–G). We considered that progression into G2 may be blocked in the absence of *ais*, precluding expression of CycB. To monitor the cell cycle, we used the Fluorescence Ubiquitin-based Cell Cycle Indicator (FUCCI) system. *Drosophila* FUCCI utilizes a GFP-tagged degron from E2f1 to mark G2, M, and G1 phases and an RFP-tagged degron from CycB to mark S, G2, and M phases (Zielke et al., 2014). We observed cells in different cell cycle stages in both WT and *bam* GKD germaria, but the *ais* GKD germaria expressed neither GFP nor RFP (Figure S3H–J"). Double negative reporter expression is thought to indicate early S phase, when expression of E2f1 is low and CycB is not expressed (Hinnant et al., 2017). The inability to express FPs is not due to a defect in translation as *ais* GKD germline can express GFP that is not tagged with the degron (Figure S3K). Taken together, we infer that loss of *ais* blocks cell cycle progression around late G1 phase/early S phase and prevents progression to G2 phase, when GSCs abscise from CBs.

In mammals, cells defective for RiBi stabilize p53, which is known to impede the G1 to S transition (Agarwal et al., 1995; Senturk and Manfredi, 2013). Thus, we hypothesized that the reduced RiBi in *ais* GKD could lead to p53 stabilization. To test this hypothesis, we immunostained for p53 and Vasa. A hybrid dysgenic cross that expresses p53 in undifferentiated cells was utilized as a positive control, and *p53* null flies were used as negative control (Figure S3L–M) (Moon et al., 2018). In WT, we observed p53 expression in the meiotic stages but p53 expression in GSCs and CBs was attenuated as previously reported (Figure 3G–G") (Lu et al., 2010). However, compared to WT GSCs/CBs, we

observed p53 expression in the stem-cysts of the *ais, ath* and *pths* GKD germlines (Figure 3G–I, Figure S3N–O), supporting the hypothesis that reduced RiBi stabilizes p53.

To determine if p53 stabilization promotes cell cycle arrest in *ais*, *ath*, and *pths* GKD to cause stem-cyst formation, we performed *ais*, *ath* and *pths* GKD in *p53* mutants. We observed a partial but significant alleviation of the cyst phenotype, such that spectrosomes were restored (Figure 3J–L, Figure S3P–T). This finding indicates that p53 contributes to cytokinesis failure upon *ais, ath* and *pths* GKD, but that additional factors are also involved. To determine if aberrant expression of p53 is sufficient to cause the formation of stem-cysts, we overexpressed (OE) p53 in the germline under the control of a UAS/GAL4 system. While 84% of germaria had a complete loss of germline as previously reported (Bakhrat et al., 2010), 12% of germaria contained germ cells that were connected by a fusome-like structure proximal to the niche, phenocopying loss of *ais*, *ath*, or *pths* (Figure 3M–N), and in the rest, we observed several single cells, compared to the control (n=55, Fisher's exact test, $p<0.001$). Taken together, we find that *ais, ath, and pths* GKD germ cells display reduced RiBi, aberrant expression of p53 protein, and a block in cell cycle progression. Reducing p53 partially alleviates GSC cytokinesis defect, while OE of p53 results in loss of germline and cytokinesis defects in the GSCs.

## Ais promotes translation of Non1, a negative regulator of p53, linking RiBi to the cell cycle

Although p53 protein levels were elevated upon *ais* GKD, *p53* mRNA levels were not significantly altered ($\log_2$ fold change: −0.49; FDR: 0.49) (Supplemental Table 3). Given that RiBi is affected, we considered that translation of p53 or one of its regulators was altered in the germline of *ais* GKD. To test this hypothesis, we performed polysome-seq of gonads enriched for GSCs or CBs as developmental controls, as well as gonads with *ais* GKD (Flora et al., 2018b). We plotted the ratios of polysome-associated RNAs to total RNAs (Figure 4A–A", Supplemental Table 4). We identified 87 mRNAs that were less efficiently translated in *ais* GKD compared to developmental controls. Loss of *ais* reduced the levels of these 87 down-regulated transcripts in polysomes, without significantly affecting their total mRNA levels (Figure 4B, Figure S4A–A'). The regulation of these 87 mRNAs are not directly mediated by Ais binding as none of the RNAs are directly bound by Ais as measured by mRNA IP-seq using Ais::GFP::3XFLAG (Supplemental Table 5). Of the 87 targets, 85 of the transcripts encode proteins associated with translation including RPs (Figure 4C). To validate that Ais regulates translation of these mRNAs, we utilized a reporter line for the Ais-regulated gene encoding Ribosomal protein S2 (RpS2) that is under endogenous control (Buszczak et al., 2007). We observed reduced levels of RpS2::GFP in the germline of *ais* GKD as well *bam*, *ais* double GKD but not *bam* GKD alone (Figure 4D–F, Figure S4B–D). To determine if reduced RpS2::GFP levels are due to a global decrease in translation, we visualized global nascent translation using O-propargyl-puromycin (OPP) that is incorporated into nascent polypeptides and can be detected (Sanchez et al., 2016). We observed that OPP incorporation, in the germline of *ais* GKD, was not reduced compared to single cells of control ovaries or *bam* GKD (Figure 4G–J). Thus, loss of *ais* results in reduced translation of a subset of transcripts.

None of these 87 targets have been directly implicated in controlling abscission (Mathieu et al., 2013; Matias et al., 2015). However, one of the targets, was an mRNA encoding Novel Nucleolar protein 1 (Non1/CG8801) (Figure 4C). The human ortholog of Non1 is GTP Binding Protein 4 (GTPBP4); these proteins are known to physically interact with p53 in both *Drosophila* and human cells and have been implicated in repressing p53 (Li et al., 2018; Lunardi et al., 2010). To determine if the protein level of Non1 is reduced upon *ais* GKD, we monitored the abundance of Non1::GFP, a transgene under endogenous control (Sarov et al., 2016). We found that Non1::GFP was expressed in the GSCs and CBs of WT (Figure 5A–A", Figure S5A–B), but was reduced in the *ais*, *ath* or *pths* GKD stem-cysts (Figure 5B–D, Figure S5C–F), suggesting that efficient RiBi promotes efficient translation of Non1.

During oogenesis, p53 is expressed in cyst stages in response to recombination-induced double strand breaks (Lu et al., 2010). We found that Non1 was highly expressed at undifferentiated stages and in two- and four-cell cysts when p53 protein levels were low, whereas its expression was attenuated at eight- and 16-cell cyst stages when p53 protein levels were high (Figure 5A–A", Figure S5A–B'). Non1 was highly expressed in egg chambers, which express low levels of p53 protein, suggesting that Non1 could regulate p53 protein levels. To determine if Non1 regulates GSC differentiation and p53, we performed *Non1* GKD and found that *Non1* GKD results in stem-cyst formation and loss of later stages, as well as increased p53 expression (Figure 5E–F', H, Figure S5G–I). In addition, we found that loss of *p53* from *Non1* GKD germaria partially suppressed the phenotype (Figure 5F–H). Thus, *Non1* is regulated by *ais* and is required for *p53* suppression and GSC abscission.

To determine if Ais, Ath, and Pths promote GSC differentiation via translation of Non1, we restored *Non1* expression in *ais*, *ath*, or *pths* GKD ovaries. We cloned *Non1* under the control of the UAS/GAL4 system (see Methods) (Rørth, 1998). While OE of Non1 alone did not cause any observable defect, restoring *Non1* expression in the *ais*, *ath*, or *pths* GKD germline significantly attenuated stem-cyst formation and increased the number of cells with spectrosomes (Figure 5I-L, Figure S5J–N). Taken together, we conclude that Non1 can partially suppress the cytokinesis defect caused by *ais*, *ath*, or *pths* GKD.

## Ais-regulated targets contain a TOP motif in their 5'UTR

We next asked how *ais* and efficient RiBi promote the translation of a subset of mRNAs, including *Non1*. We hypothesized that the 87 mRNA targets share a property that make them sensitive to RiBi. To identify shared characteristics, we performed *de novo* motif discovery of target genes compared to non-target genes (Bailey et al., 2006) and identified a polypyrimidine motif in 95% of 5'UTRs of target genes (UCUUU; E-value: $6.6e^{-094}$). This motif resembles the previously described TOP motif at the 5' end of mammalian transcripts (Philippe et al., 2018; Thoreen et al., 2012). Although the existence of TOP-containing mRNAs in *Drosophila* has been proposed, to our knowledge their presence has not been explicitly demonstrated (Chen and Steensel, 2017; Qin et al., 2007). This motivated us to precisely determine the 5' end of transcripts, so we analyzed previously published cap analysis of gene expression sequencing (CAGE-seq) data that had determined transcription

start sites (TSS) in total mRNA from the ovary (Figure 6A) (Boley et al., 2014; Chen et al., 2014). Of the 87 target genes, 76 had sufficient expression in the CAGE-seq dataset to define their TSS. We performed motif discovery using the CAGE-seq data and found that 72 of 76 Ais-regulated mRNAs have a polypyrimidine motif that starts within the first 50 nt of their TSS (Figure 6B–C, Supplemental Table 6). In mammals, it was previously thought that the canonical TOP motif begins with an invariant 'C' (Meyuhas, 2000; Philippe et al., 2020). However, systematic analysis of the sequence required for an mRNA to be regulated as a TOP containing mRNA revealed that TOP mRNAs can start with either a 'C' or a 'U' (Philippe et al., 2020). Thus, mRNAs whose efficient translation is dependent on *ais* share a terminal polypyrimidine-rich motif in their 5'UTR that resembles a TOP motif.

In vertebrates, canonical TOP-regulated mRNAs encode RPs and translation initiation factors that are coordinately regulated in response to growth cues primarily mediated by mTORC1 (Hornstein et al., 2001; Iadevaia et al., 2014; Meyuhas and Kahan, 2015) Indeed, 76 of the 87 Ais targets were RPs, and 9 were known or putative translation factors, consistent with TOP-containing mRNAs in vertebrates (Figure 4C, Supplemental Table 6). To determine if the putative TOP motifs that we identified are sensitive to TORC1 activity, we designed TOP reporter constructs. Specifically, the germline-specific *nanos* promoter was employed to drive expression of an mRNA with 1) the 5'UTR of the *ais* target *RpL30*, which contains a putative TOP motif, 2) the coding sequence for a GFP-HA fusion protein and 3) a 3'UTR (K10) that is not translationally repressed (Flora et al., 2018b; Serano et al., 1994), referred to as the WT-TOP reporter (Figure 6D). As a control, we created a construct in which the polypyrimidine sequence was mutated to a polypurine sequence referred to as the MUT-TOP reporter (Figure 6D).

In *Drosophila*, TORC1 activity increases during cyst stages (Wei et al., 2019, 2014). We found that the WT-TOP reporter is highly expressed in 8-cell cysts, whereas the MUT-TOP reporter did not (Figure 6E–F"), suggesting that the WT-TOP reporter is sensitive to TORC1 activity. Moreover, depletion of *Nitrogen permease regulator-like 3* (*Nprl3*), an inhibitor of TORC1 (Wei et al., 2014), led to a significant increase in expression of the WT-TOP reporter but not the MUT-TOP reporter (Figure S6A–E). Additionally, to attenuate TORC1 activity, we performed *raptor* GKD, one of the subunits of TORC1 (Hong et al., 2012; Loewith and Hall, 2011). We found that the WT-TOP reporter had a significant decrease in reporter expression while the MUT-TOP reporter did not (Figure S6F–J). Taken together, our data suggest that Ais-regulated transcripts contain TOP motifs that are sensitive to TORC1 activity. However, the WT-TOP reporter did not recapitulate the pattern of Non1::GFP expression, suggesting that Non1 may have additional regulators that modulate its protein levels in the cyst stages.

TOP mRNAs show increased translation in response to TORC1 signaling, leading to increased RiBi (Jefferies et al., 1997; Jia et al., 2021; Thoreen et al., 2012). However, to our knowledge, whether reduced RiBi can coordinately diminish the translation of TOP mRNAs to lower RP production to balance the levels of the distinct components needed for ribosome assembly is not known. To address this question, we crossed the transgenic flies carrying the WT-TOP reporter and MUT-TOP reporter into *bam* and *ais*, *ath*, and *pths* GKD backgrounds. We found that the expression from the WT-TOP reporter was reduced more

than mutated-TOP reporter of *ais, ath* and *pths* GKD ovaries compared to *bam* GKD ovaries (Figure 6G–H', K, Figure S6K–Q). This suggests that the TOP motif-containing mRNAs are sensitive to RiBi.

## Larp binds TOP sequences in *Drosophila*

Next, we sought to determine how TOP-containing mRNAs are regulated downstream of Ais. In mammalian cells, Larp1 is a negative regulator of TOP-containing RNAs during nutrient deprivation (Berman et al., 2020; Fonseca et al., 2015; Philippe et al., 2020). Therefore, we hypothesized that *Drosophila* Larp reduces the translation of TOP-containing mRNAs when RiBi is reduced upon loss of *ais*. First, using an available gene-trap line in which Larp is tagged with GFP and 3XFLAG, we confirmed that Larp was expressed throughout all stages of oogenesis including in GSCs (Figure S7A–A').

Next, we performed electrophoretic mobility shift assays (EMSA) to examine protein-RNA interactions with purified *Drosophila* Larp-DM15, the conserved domain that binds to TOP sequences in vertebrates (Lahr et al., 2017). As probes, we utilized capped 42-nt RNAs corresponding to the 5'UTRs of *RpL30* and *Non1*, including their respective TOP sequences. We observed a gel shift with these RNA oligos in the presence of increasing concentrations of Larp-DM15 (Figure 7A–A', Figure S7B), and this shift was abrogated when the TOP sequences were mutated to purines (Figure S7C–C'). To determine if Larp interacts with TOP-containing mRNAs *in vivo*, we immunopurified Larp::GFP::3XFLAG from the ovaries of the gene-trap line and performed RNAseq (Figure S7D). We uncovered 156 mRNAs that were bound to Larp, and 84 of these were among the 87 *ais* translationally regulated targets, including *Non1*, *RpL30*, and *RpS2* (Figure 7B–C, Supplemental Table 7). Thus, *Drosophila* Larp binds to TOP sequences *in vitro* and TOP-containing mRNAs *in vivo*.

To test our hypothesis that *Drosophila* Larp inhibits the translation of TOP-containing mRNAs upon depletion of *ais*, we immunopurified Larp::GFP::3XFLAG from *bam* and *ais* GKD ovaries. Larp was not a target of Ais either from RNAseq nor from polysome-seq (Supplemental Table 2–4). Consistent with this observation, we found that Larp protein is not expressed at higher levels in *ais* GKD compared to developmental control *bam* GKD (Figure S7E–G, Figure S7H–I). We found that Larp binding to *ais* target mRNAs *Non1* and *RpL30* was increased in *ais* GKD ovaries compared to *bam* GKD ovaries (Figure 7D, Figure S7J). In contrast, a non-target mRNA that does not contain a TOP motif, *α-tubulin* mRNA, did not have a significant increase in binding to Larp in *ais* GKD ovaries compared to *bam* GKD ovaries (Figure 7D, Figure S7J). Overall, these data suggest that reduced RiBi upon loss of *ais* increases Larp binding to the TOP-containing mRNAs *Non1* and *RpL30*.

If loss of *ais* inhibits the translation of TOP-containing mRNAs due to increased binding of Larp to its targets, then OE of Larp should phenocopy *ais* GKD. Therefore, we overexpressed the DM15 domain of Larp that we showed binds the *RpL30* and *Non1* TOP motifs *in vitro* (Figure 7A–A'), and, based on homology to mammalian Larp1, lacks the majority of the putative phosphorylation sites which regulate Larp activity (Jia et al., 2021; Lahr et al., 2017; Philippe et al., 2018). We found that OE of a Larp-DM15::GFP fusion in the germline resulted in fusome-like structures extending from the niche (Figure

7E–F'). Additionally, ovaries overexpressing Larp-DM15 had 32-cell egg chambers, which is emblematic of cytokinesis defects that occur during early oogenesis, compared to control ovaries (Figure S7K–K') (Mathieu et al., 2013; Matias et al., 2015; Sanchez et al., 2016). Our findings indicate that OE of Larp partially phenocopies *ais* GKD.

## Discussion

During *Drosophila* oogenesis, efficient RiBi is required in the germline for proper GSC cytokinesis and differentiation. The outstanding questions that needed to be addressed were: 1) Why does disrupted RiBi impair GSC abscission? And 2) How does the GSC monitor and couple RiBi to differentiation? Our results suggest that a germline RiBi defect stalls the cell cycle, resulting a loss of differentiation and the formation of stem-cysts. We discovered that proper RiBi is monitored through a translation control module that allows for co-regulation of RPs and a p53 repressor. Ais, Ath and Pths support RiBi and allowing for translation of a p53 repressor, preventing p53 stabilization, cell cycle arrest and loss of stem cell differentiation.

The developmental upregulation of p53 during GSC differentiation concomitant with reduced RiBi parallels observations in disease states, such as ribosomopathies (Calo et al., 2018; Pereboom et al., 2011; Deisenroth and Zhang, 2010). We find that p53 levels in GSCs are regulated by the conserved p53 regulator Non1. While Non1 has been shown to directly interact with p53, how it regulates p53 levels in both humans and *Drosophila* is not known (Li et al., 2018; Lunardi et al., 2010).

TOP-containing mRNAs are known to be coregulated to coordinate ribosome production in response to environmental cues (Kimball, 2002; Meyuhas and Kahan, 2015; Tang et al., 2001). Surprisingly, our observation that loss of *ais* reduces translation, albeit indirectly via regulation of RiBi, of a cohort of TOP-containing mRNAs, including Non1, suggests that the TOP motif also sensitizes their translation to lowered levels of RiBi. This notion is supported by TOP reporter assays demonstrating that reduced translation upon loss of *ais* requires the TOP motif. We hypothesize that limiting TOP mRNA translation lowers RP production to maintain a balance with reduced rRNA production. This feedback mechanism would prevent the production of excess RPs that cannot be integrated into ribosomes and the ensuing harmful aggregates (Tye et al., 2019).

The translation and stability of TOP-containing mRNAs are mediated by Larp1 and its phosphorylation (Berman et al., 2020; Hong et al., 2017; Jia et al., 2021). We found that perturbing rRNA production and thus RiBi, without directly targeting RPs, also results in dysregulation of TOP mRNAs. Our data show that *Drosophila* Larp binds the *RpL30* and *Non1* 5'UTR in a TOP-dependent manner *in vitro* and to 97% of the translation targets we identified *in vivo*. Together these data suggest that rRNA production regulates TOP mRNAs via Larp albeit indirectly. Furthermore, the cytokinesis defect caused by OE of Larp-DM15 in the germline suggests that Larp regulation could maintain the homeostasis of RiBi by balancing the expression of RP production with the rate of other aspects of RiBi, such as rRNA processing, during development.

Ribosomopathies arise from RiBi defects (Armistead and Triggs-Raine, 2014). The underlying mechanisms of tissue specificity remain unresolved. Here, we demonstrate that loss of proteins involved in rRNA processing lead to cell cycle arrest. Given that *Drosophila* GSCs undergo an atypical cell cycle as a normal part of their development it may be that this underlying cellular program in the germline leads to the tissue-specific phenotype of stem-cyst formation (Sanchez et al., 2016). This model implies that other tissues would likewise exhibit tissue-specific manifestations of ribosomopathies due to their underlying cell state. Our data suggests two other sources of potential tissue specificity: 1) tissues express different cohorts of mRNAs, such as *Non1*, that are sensitive to ribosome levels. 2) p53 activation, as previously described, is differentially tolerated in different tissues (Bowen and Attardi, 2019; Calo et al., 2018; Jones et al., 2008). Together, these mechanisms could begin to explain the tissue-specific nature of ribosomopathies and their link to differentiation.

### Limitations of the Study

The exact processing steps that Ais, Ath, and Pths promote in *Drosophila* RiBi remain unknown; we hypothesize that the processing step they act on the rRNA would be similar to what has been reported in yeast and mammals (Granneman et al., 2006; Sekiguchi et al., 2006; Tafforeau et al., 2013). Lack of a full rescue from *ais*, *ath*, and *pths* GKD in *p53* mutants suggest that multiple genes likely influence the cell cycle arrest. Finally, it is possible that the roles of Ais, Ath, and Pths in indirectly promoting Non1 translation does not represent a general effect of RiBi defects and is specific to these three proteins. However, we think this is unlikely as nearly all genes involved in RiBi outside of RPs share the same phenotype when depleted during *Drosophila* oogenesis.

## STAR Methods

### Resource Availability

**Lead Contact:** Further information and requests for resources and reagents should be directed to and will be fulfilled by the lead contact, Prashanth Rangan (prangan@albany.edu).

**Materials availability:** Materials generated during this study are available upon request.

**Data and Code availability:** Sequencing data generated during this study are available on GEO under the accession GSE171350. Other data generated during this study are available from the lead contact. Any additional information required to reanalyze the data reported in this paper is available from the lead contact upon request. This study did not generate any code.

### Experimental model and subject details

All strains used in this study are listed in the key resources table Drosophila were raised on corn flour and agar media with brewer’s yeast at 18–29°C and females were dissected between 1–3 days post-eclosion.

## Method Details

**Protein Domain Analysis:** Protein domain figures were adapted from: The Pfam protein families database in 2019: S. ElGebali et al. Nucleic Acids Research (2019). Protein Similarity values were obtained from the DRSC/TRiP Functional Genomics Resources.

**Protein Conservation Analysis:** Evolutionary trees were generated using MEGA. The evolutionary history was inferred by using the Maximum Likelihood method and JTT matrix-based model. The tree with the highest log likelihood is shown. Initial tree(s) for the heuristic search were obtained automatically by applying Neighbor-Join and BioNJ algorithms to a matrix of pairwise distances estimated using a JTT model, and then selecting the topology with superior log likelihood value. Trees are drawn to scale, with branch lengths measured in the number of substitutions per site.

**TOP Reporter Cloning—**Gene blocks (Supplemental Table 8) were cloned into pCasper2 containing a Nos promoter, HA-tag, GFP-tag, and K10 3'UTR. PCR was used in order to amplify the gene block and to remove the 5'-end of the RpL30 5'UTR in order to generate the 5'-UTR discovered via CAGE-seq. In order to clone the Nos promoter followed by the RpL30 5'UTR without an intervening restriction site, the portion of the plasmid 5' of the 5'UTR consisting of a portion of the plasmid backbone, a NotI restriction site, and the Nos Promoter was amplified from the pCasper plasmid using PCR. HiFi cloning was performed on the amplified fragments. The backbone was cut with NotI and SpeI and HiFi cloning was performed according to the manufactures' instructions except the HiFi incubation was performed for 1 hour to increase cloning efficiency. Colonies were picked and cultured and plasmids were purified using standard techniques. Sequencing was performed by Eton Bioscience Inc. to confirm the correct sequence was present in the final plasmids. Midi-prep scale plasmid was prepared using standard methods and plasmids were sent to BestGene Inc. for microinjection.

**Gateway Cloning—**Gateway cloning was performed as described according to the manufacture's manual. Briefly, primers containing the appropriate Gateway *attb* sequence on the 5'-ends and gene specific sequences on the 3'-ends (Supplemental Table 8) were used to PCR amplify each gene of interest. PCR fragments were BP cloned into pEntr221 as detailed in the Thermofisher Gateway Cloning Manual and used to transform Invitrogen One Shot OmniMAX 2 T1 Phage-Resistant Cells. Resulting clones were picked and used to perform LR cloning into either pPGW or pPWG as appropriate. Cloning was carried out according to the Thermofisher Gateway Cloning Manual except the LR incubation was carried out up to 16 hours. Colonies were picked and cultured and plasmids were purified using standard techniques. Sequencing was performed by Eton Bioscience Inc. to confirm the correct sequence was present in the final plasmids. Midi-prep scale plasmid was prepared using standard methods and plasmids were sent to BestGene Inc. for microinjection.

**Egg Laying Test—**Newly eclosed flies were collected and fattened overnight on yeast. Six female flies were crossed to 4 male controls and kept in cages at 25°C. Flies were allowed to lay for three days, and plates were changed and counted daily. Total number of eggs laid

over the three day laying periods were determined and averaged between three replicate crosses for control and experimental crosses.

**Immunostaining—**Ovaries were dissected and teased apart with mounting needles in cold PBS and kept on ice for subsequent dissections. All incubations were performed with nutation. Ovaries were fixed for 10–15 min in 5% methanol-free formaldehyde in PBS. Ovaries were washed with PBT (1x PBS, 0.5% Triton X-100, 0.3% BSA) once quickly, twice for 5 min, and finally for 15 min. Ovaries were incubated overnight, up to 72 hours in PBT with the appropriate primary antibodies. Primary antibodies were used at the concentration indicated: mouse anti-1B1 1:20 (DSHB 1B1), rabbit anti-Vasa 1:833–1:4000 (Rangan Lab), chicken anti-Vasa 1:833–1:4000 (Rangan Lab) (Upadhyay et al., 2016), rabbit anti-pTyr 1:500 (Sigma T1235), rabbit anti-pMad 1:200 (Abcam ab52903), rabbit anti-GFP 1:2000 (abcam, ab6556), mouse anti-p53 1:200 (DSHB 25F4), Rabbit anti-CycB 1:200 (Santa Cruz Biotechnology, 25764), Rabbit anti-Fibrillarin 1:200 (Abcam ab5821), Mouse anti-Fibrillarin 1:50 (Fuchs Lab) (McCarthy et al., 2018). Ovaries were again washed with PBT once quickly, twice for 5 min, and finally for 15 min. Ovaries were then incubated with the appropriate secondary antibodies in PBT overnight up to 72 hours at 4°C. Secondary antibodies were used at a dilution of 1:500. Ovaries were washed once quickly, twice for 5 min, and finally for 15 min in PBST (1x PBS, 0.2% Tween 20 Ovaries). Ovaries were mounted with Vectashield with 4′,6-diamidino-2-phenylindole (DAPI) (Vector Laboratories) and imaged on a Zeiss 710. All gain, laser power, and other relevant settings were kept constant for any immunostainings being compared. Image processing was performed in Fiji, gain was adjusted, and images were cropped in Photoshop CC 2018.

**Fluorescent Imaging—**Tissues were visualized and imaged were acquired using a Zeiss LSM-710 confocal microscope under the 20× and 40× oil objectives.

**Measurement of global protein synthesis—**OPP (Thermo Fisher, C10456) treatment was performed as in McCarthy (2019). Briefly, ovaries were dissected in Schneider's media (Thermo Fisher, 21720024) and incubated in 50 μM of OPP reagent for 30 minutes. Tissue was washed in 1x PBS and fixed for 10 minutes in 1x PBS plus 5% methanol-free formaldehyde. Tissue was permeabilized with 1% Triton X-100 in 1x PBST (1x PBS, 0.2% Tween 20) for 30 minutes. Samples were washed with 1x PBS and incubated with Click-iT reaction cocktail, washed with Click-iT reaction rinse buffer according to manufacturer's instructions. Samples were then immunostained according to previously described procedures.

**Image Quantifications—**All quantifications were performed on images using the same confocal settings. A.U. quantifications were performed in Fiji on images taken with identical settings using the "Measure" function. Intensities were normalized as indicated in the figure legends, boxplots of A.U. measurements were plotted using R and statistics were calculated using R.

Quantification of nucleolar size was measured in Fiji by measuring the diameter of the nucleolus using the measure tool in Fiji. Volumes were calculated using the formula for a sphere.

Quantification of p53 area of expression was performed from control, *nosGAL4* and nosGAL4>*ais* RNAi germaria. A manual threshold was set based off of qualitative assessment of a “punctate”. For control ovaries, cells proximal to the niche consisting of GSCs/CBs were outlined and for *ais* RNAi the entire germline proximal to the niche was outlined and a Fiji script was used to determine the number of pixels above the threshold and the total number of pixels. Data from each slice for each replicate was summed prior to plotting and statistical analysis.

Colocalization analysis of DExD/H-box proteins with Fibrillarin was performed in Fiji using the Plot Profile tool. A selection box was drawn over a Fibrillarin punctate of interest (indicated with a box in the images) and Plot Profiles was acquired for each channel of interest. Data was plotted and Spearman correlations calculated using R.

Quantification of Non1::GFP expression and p53 expression over development was calculated in Fiji using the Auto Threshold tool with the Yen method (Sezgin and Sankur, 2004) to threshold expression. Quantifications were performed on 3 merged slices and egg chambers were cropped out of quantified images prior to thresholding to prevent areas outside of the germarium from influencing the thresholding algorithm. Areas of germline with “high” and “low” expression of Non1-GFP were outlined manually and a custom Fiji script was used in order to quantify the proportion of pixels in the selected marked as positive for expression for either Non1-GFP or p53, staging was inferred from the results of the Non1-GFP quantification performed using 1B1 to determine the stages of peak Non1 expression. Percent area was plotted with ggplot2 as boxplots in a custom R script.

**RNA Extraction from Ovaries—**RNA extraction was performed using standard methods. Ovaries were dissected into PBS and transferred to microcentrifuge tubes. PBS was removed and 100ul of Trizol was added and ovaries were flash frozen and stored at −80 °C. Ovaries were lysed in the microcentrifuge tube using a plastic disposable pestle. Trizol was added to 1 mL total volume and sample was vigorously shaken and incubated for 5 min at RT. The samples were centrifuged for x min at >13,000 g at 4 °C and the supernatant was transferred to a fresh microcentrifuge tube. 500 ul of chloroform was added and the samples were vigorously shaken and incubated for 5 minutes at RT. Samples were spun at max speed for 10 minutes at 4 °C. The supernatant was transferred to a fresh microcentrifuge tube and ethanol precipitated. Sodium acetate was added equaling 10% of the volume transferred and 2–2.5 volumes of 100% ethanol were added. The samples were shaken thoroughly and left to precipitate at −20 °C overnight. The samples were centrifuged at max speed at 4 °C for 15 min to pellet the RNA. The supernatant was discarded and 500 ul of 75% ethanol was added to wash the pellet. The samples were vortexed to dislodge the pellet to ensure thorough washing. The samples were spun at 4 °C for 5 min and the supernatant was discarded. The pellets were left for 10–20 min until dry. The pellets were resuspended in 20–50ul of RNAse free water and the absorbance at 260 was measured on a nanodrop to measure the concentration of each sample.

**S2 Cell RNAi—**DRSC-S2 cells (Stock #181, DGRC) were cultured according to standard methods in M3+BPYE media supplemented with 10% heat-inactivated FBS. dsRNA for RNAi was prepared as described by the SnapDragon manual. Briefly, template was prepared from S2 cell cDNA using the appropriate primers (see primer list) designed using SnapDragon (https://www.flyrnai.org/snapdragon). Template was either used directly for *in-vitro* transcription or TA-cloned into the pCR2.1-TOPO vector (K450002) followed by transformation into TOP-10 cells (K450002), plasmid purified, and digested with *Eco*R I prior to *in-vitro* transcription. For *in-vitro* transcription the T7 Megascript kit (AM1334) was used following manufacturer's instructions and in-vitro transcriptions were incubated overnight at 37°C. The RNA was treated with DNAse according to the T7 Megascript manual and the RNA was purified using acid-phenol chloroform extraction and ethanol precipitated. The resulting RNA was annealed by heating at 65°C for 5 minutes and slow cooling to 37°C for an hour. S2 cell RNAi was performed essentially as previously described using Effectine (Zhou et al., 2013). $1.0\times10^6$ cells were seeded 30 minutes prior to transfection and allowed to attach. After 30 minutes, just prior to transfection, the media was changed for 500 μl of fresh media. 500 μl of transfection complexes using 1 μg of dsRNA was prepared per well of a 6-well plate and pipetted dropwise onto seeded cells. After 24 hours an additional 1 mL of media was added to each well. After an additional 24 hours cells were passaged to 10 cm dishes. After an additional 3 days cells were harvested for further analysis.

**Polysome-profiling—**Polysome-profiling in S2 cells was performed as in Fuchs et al. (2011) with minor modifications. S2 cells were resuspended by pipetting, pelleted by centrifugation at 800g for one minute, and washed in cold PBS. Cells were again pelleted and resuspended in 400 μl of lysis buffer (300 mM NaCl, 15 mM Tris-HCl, pH 7.5, 15 mM EDTA, 100 μg/mL cycloheximide, 1% Triton X-100). Cells were then allowed to continue to lyse for 15 min on ice. Lysate was cleared by centrifugation at 8500g for 5 min at 4°C. Cleared lysate was loaded onto 10%–50% sucrose gradients (300 mM NaCl, 15 mM Tris-HCl, pH 7.5, 15 mM MgCl2, 100 g/mL cycloheximide) and centrifuged in an SW41 rotor at 35,000 RPM, for 3 hours. Gradients were fractionated on a Density Gradient Fractionation System (Brandel, #621140007) at 0.75 mL/min. Data generated from gradients were plotted using R.

**Western Blot—**Western blotting was performed according to standard methods, briefly, each sample was loaded onto a 4–20% commercial, precast gels and run at 100V for 60–90m depending on the size of the protein of interest. Gels were transferred to nitrocellulose membranes at 100V for 1hr at 4°C. Blot was blocked in 1% milk in PBS and washed 3 times with PBS-T for 5 minutes. Conjugated primary Mouse anti-FLAG-HRP 1:5000 (Sigma Aldrich, A8592) was diluted in PBS-T+5% BSA and incubated overnight. Blot was washed once quickly, once for 5m, and once for 10m in PBS-T. Blot was subsequently imaged with ECL. Blot was washed once quickly, once for 5m, and once for 10m in PBS-T and imaged.

**mRNAseq Library Preparation and Analysis—**Libraries were prepared with the Biooscientific kit (Bioo Scientific Corp., NOVA-5138-08) according to manufacturer's instructions with minor modifications. Briefly, RNA was prepared with Turbo DNAse

according to manufacturer's instructions (TURBO DNA-free Kit, Life Technologies, AM1907), and incubated at 37°C for 30 min. DNAse was inactivated using the included DNAse Inactivation reagent and buffer according to manufactures instructions. The RNA was centrifuged at 1000 g for 1.5 min and 19 µl of supernatant was transferred into a new 1.5 mL tube. This tube was again centrifuged at 1000 g for 1.5 min and 18 µl of supernatant was transferred to a new tube to minimize any Inactivation reagent carry-over. RNA concentration was measured on a nanodrop. Poly-A selection was performed on a normalized quantity of RNA dependent on the lowest amount of RNA in a sample, but within the manufacturer's specifications for starting material. Poly-A selection was performed according to manufacturer's instructions (Bioo Scientific Corp., 710 NOVA-512991). Following Poly-A selection mRNA libraries were generated according to manufactures instructions (Bioo Scientific Corp., NOVA-5138-08) except RNA was incubated for 13 min at 95°C to generate optimal fragment sizes. Library quantity was assessed via Qubit according to manufacturer's instructions and library quality was assessed with a Bioanalyzer or Fragment Analyzer according to manufacturer's instructions to assess the library size distribution. Sequencing was performed on biological duplicates from each genotype on an Illumina NextSeq500 by the Center for Functional Genomics (CFG) to generate single end 75 base pair reads. Reads were aligned to the dm6.01 assembly of the Drosophila genome using HISAT v2.1.0. Reads were counted using featureCounts v1.4.6.p5. UCSC genome browser tracks were generated using the bam coverage module of deeptools v3.1.2.0.0. Differential expression analysis was performed using DEseq2 (v1.24.0) and data was plotted using R. Differentially expressed genes were those with $\log_2$(foldchange) > |1.5| and FDR < 0.05 in the *ais* RNAi versus *bam* RNAi experiment and foldchange > |1.5| and FDR < 0.05 in the *bam* RNAi; *ais* RNAi versus *bam* RNAi experiment. GO-term analysis of GO biological processes was performed on differentially expressed genes using PANTHER via http://geneontology.org/. Fisher's exact test was used to calculate significance and FDR was used to correct for multiple testing. GO-term analysis results were plotted using R.

**Polysome-seq—**Polysome-seq was performed as in Flora et al. (2018b) with minor modifications. Ovaries were dissected in PBS and transferred to a microcentrifuge tube in liquid nitrogen. Ovaries were lysed in 300 µl of lysis buffer (300 mM NaCl, 15 mM Tris-HCl, pH 7.5, 15 mM EDTA, 100 µg/mL cycloheximide, 1% Triton X-100) and allowed to lyse for 15 min on ice. Lysate was cleared by centrifugation at 8500g for 5 min at 4°C. 20% of the lysate was reserved as input, 1 mL of Trizol (Invitrogen, 15596026) was added and RNA was stored at −80°C. Cleared lysate was loaded onto 10%–50% sucrose gradients (300 mM NaCl, 15 mM Tris-HCl, pH 7.5, 15 mM MgCl2, 100 g/mL cycloheximide) and centrifuged in an SW41 rotor at 35,000 RPM, for 3 hours. Gradients were fractionated on a Density Gradient Fractionation System (Brandel, #621140007) at 0.75 mL/min, 20 µl of 20% SDS, 8 µl of 0.5 M pH 8 EDTA, and 16 µl of proteinase K (NEB, P8107S) was added to each polysome fraction. Fractions were incubated for 30m at 37°C. Standard acid phenol chloroform purification followed by ethanol precipitation was performed on each fraction. The RNA from polysome fractions was pooled and RNAseq libraries were prepared.

**Polysome-seq Data Analysis—**Reads were checked for quality using FastQC. Reads were mapped to the *Drosophila* genome (dm6.01) using Hisat version 2.1.0. Mapped

reads were assigned to features using featureCount version v1.6.4. Translation efficiency was calculated as in (Flora et al., 2018; Kronja et al., 2014) using an R script. Briefly, TPMs (transcripts per million) values were calculated. Any gene having zero reads in any library was discarded from further analysis. The $\log_2$ ratio of CPMs between the polysome fraction and total mRNA was calculated and averaged between replicates. This ratio represents the TE. TE of each replicate was averaged. Targets were defined as transcripts falling greater or less than two standard deviations from the median TE in ais RNAi for upregulated and downregulated genes respectively, but not in either of the two developmental controls (nosGAL4 UAS-*tkv* or nosGAL4 UAS-*bam* RNAi). Additionally, genes were only considered targets if their mean TE value in nosGAL4 UAS-*ais* RNAi was higher (for upregulated targets) or lower (for downregulated targets) than their mean TE values in both of the two developmental controls. Finally, only targets meeting a conservative expression cutoff of $\log_2$(TPM) expression greater than five were considered to exclude more lowly expressed genes as they are highly influenced by noise in polysome-seq in both controls.

**CAGE-seq Tracks—**CAGE-seq tracks were visualized using the UCSC Genome Browser after adding the publicly available track hub ‘EPD Viewer Hub’.

**CAGE-seq Data Reanalysis—**Publicly available genome browser tracks were obtained of CAGE-seq data (generated by Chen et al. (2014) and viewed through the UCSC Genome Browser. The original CAGE-seq data from ovaries was obtained from SRA under the accession number SRR488282. Reads were aligned to the dm6.01 assembly of the *Drosophila* genome using HISAT v2.1.0. cageFightR was used to determine the dominant TSS for every gene with sufficient expression in from the aligned dataset according to its documentation with default parameters excepting the following: For getCTSS, a mappingQualityThreshold of 10 was used. For normalizeTagCount the method used was “simpleTPM”. For clusterCTSS the following parameters were used; threshold = 1, thresholdIsTPM = TRUE, nrPassThreshold = 1, method = “paraclu”, maxDist = 20, removeSingletons = TRUE, keepSingletonsAbove = 5. R was used to obtain genome sequence information downstream of the TSS of each gene identified.

To generate a table of *ais* polysome-seq target 5’UTRs adjusted using CAGE-seq data, bigwig files of CAGE-seq from ovaries were obtained from EPD Viewer Hub. The most highly expressed TSS within a CAGE cluster (obtained as described in this section) was used to determine the new 5’-end coordinate associated with each *ais* polysome-seq target gene at the transcript level. These coordinates were used to obtain the corrected 5’UTR using R and transcripts with identical sequences were discarded.

**Motif Enrichment Analysis—**Initial motif discovery was performed using MEME (Bailey et al., 2006). Follow up discovery to was performed using Homer (Heinz et al., 2010) using the findmotifs.pl module, supplying Homer with the first 200 nucleotides downstream of the TSS as determined by CAGE-seq for polysome-seq targets and non-targets as a background control with the following parameters “-rna -nogo - p 6 -len 6”. Only motifs not marked as potential false positives were considered. The position of the putative TOP motifs was determined using a custom R script by searching for the first instance of

any five pyrimidines in a row within the first 200 nucleotides of the TSS using the Biostrings package (Pagès et al., 2019). Results were plotted as a histogram in R.

**RNA Immunoprecipitation (RNA IP)—**All RIPs were performed with biological triplicates. 50–60 ovary pairs were dissected for each sample in RNase free PBS and dissected ovaries were kept on ice during subsequent dissections. After dissection, ovaries were washed with 500 µl of PBS to remove any debris. This PBS was removed, and ovaries were lysed in 100 µl of RIPA buffer (10 mM Tris-Cl Buffer (pH 8.0), 1 mM EDTA, 1% Triton X-100,0.1% Sodium deoxycholate, 0.1% SDS, 140 mM NaCl, 1 mM PMSF, 1 cOmplete, EDTA-free Protease Inhibitor/10mL buffer (Roche, 11873580001), RNase free H2O) supplemented with 8 µl of RNase Out. Following lysis an additional 180 µl of RIPA was added to each sample. Lysate was cleared with centrifugation at 14,000g for 20m at 4°C. Cleared lysate was transferred to a new 1.5 mL tube. 10% of this lysate was reserved for RNA input and 5% was reserved as a protein input. To the RNA input 100 µl of Trizol was added and the input was stored at −80°C. To the protein input SDS loading buffer was added to a 1X working concentration and the sample was heated at 95°C for 5m and stored at −20°C. The remaining lysate was equally divided into two new 1.5 mL tubes. To one tube 3 µg of mouse anti-FLAG antibody (Sigma Aldrich, F1804) was added and to the other tube 3 µg of mouse IgG was added. These samples were incubated for 3 hours with nutation at 4°C. NP40 buffer was diluted to a 1X working concentration from a 10X stock (10x NP40 Buffer: 50 mM Tris-Cl Buffer (pH 8.0), 150 mM NaCl, 10% NP-40, 1 cOmplete, EDTA-free Protease Inhibitor Cocktail Pill/10mL buffer, RNase free H2O). 30 µl of Protein-G beads per RIP were pelleted on a magnetic stand and supernatant was discarded. 500 µl of 1X NP40 buffer was used to resuspend Protein-G beads by nutation. Once beads were resuspended, they were again pelleted on the magnetic stand. This washing process was repeated a total of 5 times. Washed Protein-G beads were added to each lysate and incubated overnight. The next day fresh 1X NP40 buffer was prepared. Lysates were pelleted on a magnetic stand at 4°C and supernatant was discarded. 300 µl of 1X NP40 buffer was added to each sample and samples were resuspended by nutation at 4°C. Once samples were thoroughly resuspended, they were pelleted on a magnetic stand. These washing steps were repeated 6 times. Following the final washing steps, beads were resuspended in 25 ul of 1X NP40 Buffer. 5 µl of beads were set aside for Western and the remaining beads were stored at −80°C in 100 µl of Trizol. SDS loading buffer was added was added to a 1X working concentration and the sample was heated at 95°C for 5m and stored at −20°C or used for Western (refer to Western Blot section).

**RNA IPseq—**RNA was purified as previously described. RNA yield was quantified using Qubit or nanodrop according to manufactures instructions. RNA was run on a Fragment Analyzer according to manufactures instructions to assess quality. Inputs were diluted 1:50 to bring them into a similar range as the IgG and IP samples. To each sample 0.5 ng of Promega Luciferase Control RNA was added as a spike-in. Libraries were prepared as previously described except Poly(A) selection steps were skipped and library preparation was started with between 1–100 ng of total RNA. Reads were mapped to the M21017.1 NCBI *Drosophila* rRNA sequence record and the sequence of Luciferase obtained from Promega. All further analysis was performed using custom R scripts. Reads were assigned

to features using featureCounts based off of a custom GTF file assembled based off of the Flybase record of rRNA sequences. Reads mapping to rRNA were normalized to reads mapping to the Luciferase spike-in control. Reads were further normalized to the reads from the corresponding input library to account for differences in input rRNA concentration between replicates and replicates were subsequently averaged. Tracks were visualized using the R package 'ggplot2', with additional formatting performed using 'scales' and 'egg'. The rRNA GTF was read into R using 'rtracklayer' and visualized using 'gggenes'. Average reads mapping to rRNA from IgG control and IP was plotted and a one-sided bootstrapped paired t-test for was performed on regions on rRNA that appeared to be enriched in the IP samples compared to the IgG control as it is a non-parametric test suitable for use with low n using R with 100,000 iterations.

## Larp Gel Shifts

**Cloning, Protein expression and purification:** The Larp-DM15 protein expression construct (amino acids 1330–1481 corresponding to isoform D) was cloned into a modified pET28a vector by PCR using cDNA corresponding to accession ID NP_733244.5. The resulting fusion protein has an N-fHis$_{10}$-maltose binding protein (MBP)-tobacco etch virus (TEV) protease recognition site tag. Protein expression and purification were performed as described previously (Lahr et al., 2015). Briefly, plasmid was transformed into BL21(DE3) *E. coli* cells and plated onto kanamycin-supplemented agar plates. A confluent plate was used to inoculate 500 mL of autoinduction media (Studier, 2005). Cells were grown for three hours at 37°C and induced overnight at 18°C. Cells were harvested, flash frozen, and stored at −80°C.

Cells were resuspended in lysis buffer (50 mM Tris, pH 8, 400 mM NaCl, 10 mM imidazole, 10% glycerol) supplemented with aprotinin (Gold Bio), leupeptin (RPI Research), and PMSF (Sigma) protease inhibitors. Cells were lysed via homogenization. Lysate was clarified by centrifugation and incubated with Ni-NTA resin (ThermoScientific) for batch purification. Resin was washed with lysis buffer supplemented with 35 mM imidazole to remove non-specific interactions. His$_{10}$-MBP-DM15 was eluted with 250 mM imidazole. The tag was removed via proteolysis using TEV protease and simultaneously dialyzed overnight (3 mg TEV to 40 mL protein elution). Larp-DM15 was further purified by tandem anion (GE HiTrap Q) and cation exchange (GE HiTrap SP) chromatography using an AKTA Pure (GE) to remove nucleic acid and protein contaminants. The columns were washed with in buffer containing 50 mM Tris, pH 7, 175 mM NaCl, 0.5 mM EDTA, and 10% glycerol and eluted with a gradient of the same buffer containing higher salt (1 M NaCl). Fractions containing Larp-DM15 were pooled, and 3 M ammonium sulfate was added to a final concentration of 1 M. A butyl column (GE HiTrap Butyl HP) was run to remove TEV contamination. The wash buffer contained 50 mM Tris, pH 7, 1 M ammonium sulfate, and 5% glycerol, and the elution buffer contained 50 mM Tris pH 7 and 2 mM DTT. Fractions containing Larp-DM15 were buffer exchanged into storage buffer (50 mM Tris pH, 7.5, 250 mM NaCl, 2 mM DTT, 25% glycerol), flash frozen in liquid nitrogen, and stored at −80°C. The purification scheme and buffer conditions were the same as with *Hs*DM15 (Lahr et al., 2015), except cation and anion exchange buffers were at pH 7, as noted above.

**RNA preparation:** 5'-triphosphorylated *RpL30* and *Non1* 42-mers were synthesized (ChemGenes). Purine-substituted controls were synthesized by *in vitro* transcription using homemade P266L T7 RNAP polymerase (Guillerez et al., 2005). The transcription reaction containing 40 mM Tris, pH 8, 10 mM DTT, 5 mM spermidine, 2 mM NTPs, and 10–15 mM $MgCl_2$ was incubated at 37°C for 4 hours. Transcripts were subsequently purified from an 8% polyacrylamide/6M urea/1XTBE denaturing gel, eluted passively using 10 mM sodium cacodylate, pH 6.5, and concentrated using spin concentrators (Millipore Amicon). All oligos were radioactively capped using Vaccinia virus capping system (NEB) and [$\alpha$–$^{32}$P]-GTP (Perkin-Elmer). Labelled oligos were purified using a 10% polyacrylamide/6M urea/1XTBE denaturing gel, eluted with 10 mM sodium cacodylate, pH 6.5, and concentrated by ethanol precipitation.

The RNA sequences used were:

RpL30: CUUUUGCCAUUGUCAGCCGACGAAGUGCUUUAACCCAAACUA

Non1: CUUUUUGGAAUACGAAGCUGACACCGCGUGGUGUUUUUGCUU

*Purine-substituted RPL30 control:
GAAAAGCCAUUGUCAGCCGACGAAGUGCUUUAACCCAAACUA

*Purine-substituted Non1 control:
GAAAAAGGAAUACGAAGCUGACACCGCGUGGUGUUUUUGCUU

Oligos used for run-off transcription

| DNA oligo | Sequence (5' to 3') |
|---|---|
| **RpL30 control gene block (with 3' HDV) | GCGCGCGAATTCTAATACGACTCACTATAGAAAAGCCATTGTCAGCC GACGAAGTGCTTTAACCCAAACTAGGGTCGGCATGGCATCTCCACCT CCTCGCGGTCCGACCTGGGCTACTTCGGTAGGCTAAGGGAGAAGCT TGGCACTGGCCGTCGTTT |
| Non1 control Forward | GCGCGCGAATTCTAATACGACTCACTATAGGAAAAAGGAATACGAAG CTGACA |
| Non1 control Reverse | AAGCAAAAACACCACGCGGTGTCAGCTTCGTATTCCTTTTTCCTATAG TGAG |
| 5' GEN amp | GCGCGCGAATTCTAATACGACTCA |
| RpL30 amp Reverse | TAGTTTGGGTTAAAGCACTTCGTCGGC |
| Non1 amp Reverse | AAGCAAAAACACCACGCGGTGTCA |

*These RNAs were synthesized using run-off transcription.

**Electrophoretic mobility shift assays (EMSAs):** Each binding reaction contained 125 total radioactive counts with final reaction conditions of: 20 mM Tris-HCl, pH 8, 150 mM NaCl, 10% glycerol, 1 mM DTT, 0.5 μg tRNA (Ambion), 1 μg BSA (Invitrogen), and <90 pM RNA. To anneal RNA, oligos were snap-cooled by heating at 95°C for 1 min and cooled on ice for 1 hour. For capped RpL30 shifts and capped purine-substituted controls, final concentrations of 0, 0.001, 0.003, 0.01, 0.03, 0.1, 0.3, 1, 3, 10, 30, and 100 nM Larp-DM15 were titrated. For capped Non1 shifts, final concentrations of 0, 0.01, 0.03, 0.1, 0.3, 1, 3, 10,

30, 100, 300, and 1000 nM Larp-DM15 were titrated. Native 7% polyacrylamide 0.5X TBE gels were pre-run on ice at 120 V for 30 min. Binding reactions were run at 120 V on ice for 45–52 min. Gels were dried for 30 min and allowed to expose overnight using a phosphor screen (GE). Screens were imaged using GE Amersham Typhoon. Bands were quantified using ImageQuant TL (GE). Background subtraction was first done using the rolling ball method and then subtracting the signal from the zero-protein lane from each of the shifted bands. Fraction shifted was determined by dividing the background-corrected intensity of the shifted band by total intensity of bands in each lane. Three independent experiments were done for each oligo, with the average plotted and standard deviation shown.

**mRNA IPseq—**IPs of Larp and Ais were performed as described in the RNA IP-seq section above in triplicate. mRNA libraries were prepared as described in mRNAseq Library Preparation and Data Processing using a constant volume of RNA from each sample with input samples having been diluted 1:50. Data was processed as described as in the mRNAseq Library Preparation and Data Processing section. Targets are defined as genes with >2 fold enrichment and an adjusted $p < 0.05$ in the Larp-IP libraries compared to input libraries, but not meeting those criteria in the IgG libraries compared to input.

**Larp RNA IP qPCR—**Larp RNA IP was performed as described in the Larp RNA IPseq section with the following modifications. As the ovaries used were small, they were flash frozen in order to accumulate 40–50 ovaries for each biological replicate. Additionally, 5% input was taken for both RNA and protein samples. Once RNA was purified all of the RNA was treated with Turbo DNAse as in the mRNAseq Library Preparation and Analysis section. Reverse transcription (RT) was performed using Superscript II according to the manufacture's protocol with equivalent volumes of RNA for each sample. cDNA was diluted 1:8 before performing qPCR using Syber Green. Each reaction consisted of 5ul Syber Green master mix, 0.4 ul water, 0.3 ul of each primer, and 4 ul of diluted cDNA (Supplemental Table 8). For each sample 3 biological and 3 technical replicates were performed. Outlier values of technical replicates were removed using a Dixon test with a cutoff of $p<0.05$. Remaining technical replicates were averaged, and the IP Input Ct value, the $\log_2$ of the Input dilution (20) was also subtracted to account for the Input being 5% of the total sample as follows:

$$\Delta Ct[\text{normalized IP}] = (\text{Average } Ct[\text{IP}] - (\text{Average } Ct[\text{Input}] - \log_2(\text{Input Dilution Factor})))$$

Next, RNA recovery was normalized using the spike-in control for each sample as follows:

$$\Delta\Delta Ct = \Delta Ct[\text{normalized IP}] - \Delta Ct[\text{Luciferase}]$$

Next, Each sample was normalized to it's matched *bam* RNAi control as follows:

$$\textit{bam}\text{ RNAi normalized } Ct = \Delta\Delta Ct[\textit{ais}\text{ RNAi IP}] - \Delta\Delta Ct[[\textit{bam}\text{ RNAi IP}]$$

Finally, fold increase of IP from *ais* RNAi over *bam* RNAi was calculated as follows:

$$\text{Fold Enrichment} = 2^{(-\textit{bam}\text{ RNAi normalized Ct})}$$

Fold enrichment was plotted and One-sample t-test performed on *ais* RNAi samples in R using a mu of 1.

### Quantification and statistical analysis

All statistical analyses were conducted in R. The specific tests, sample, size, p-value and asterisks are displayed in the corresponding legends.

## Supplementary Material

Refer to Web version on PubMed Central for supplementary material.

## Acknowledgements

We thank members of the Rangan, Fuchs labs as well as Drs. Sammons, Marlow, and Life Science Editors for their comments the manuscript. We thank the BDSC, VDRC, BDGP Gene Disruption Project, and Flybase for reagents and resources. P.R. is funded by the NIH/NIGMS (R01GM111779-06 and RO1GM135628-01), G.F. is funded by NSF MCB-2047629 and NIH RO3 AI144839, D.E.S. was funded by Marie Curie CIG 334077/IRTIM and the Austrian Science Fund (FWF) grant ASI_FWF01_P29638S, and A.B is funded by NIH R01GM116889 and American Cancer Society RSG-17-197-01-RMC.

## References

Agarwal ML, Agarwal A, Taylor WR, Stark GR, 1995. p53 controls both the G2/M and the G1 cell cycle checkpoints and mediates reversible growth arrest in human fibroblasts. Proc. Natl. Acad. Sci 92, 8493–8497. [PubMed: 7667317]

Armistead J, Triggs-Raine B, 2014. Diverse diseases from a ubiquitous process: The ribosomopathy paradox. FEBS Lett. 588, 1491–1500. 10.1016/j.febslet.2014.03.024 [PubMed: 24657617]

Bailey TL, Williams N, Misleh C, Li WW, 2006. MEME: discovering and analyzing DNA and protein sequence motifs. Nucleic Acids Res. 34, W369–W373. [PubMed: 16845028]

Bakhrat A, Pritchett T, Peretz G, McCall K, Abdu U, 2010. Drosophila Chk2 and p53 proteins induce stage-specific cell death independently during oogenesis. Apoptosis 15, 1425–1434. 10.1007/s10495-010-0539-z [PubMed: 20838898]

Berman AJ, Thoreen CC, Dedeic Z, Chettle J, Roux PP, Blagden SP, 2020. Controversies around the function of LARP1. RNA Biol 1–11. 10.1080/15476286.2020.1733787

Blagden SP, Gatt MK, Archambault V, Lada K, Ichihara K, Lilley KS, Inoue YH, Glover DM, 2009. Drosophila Larp associates with poly (A)-binding protein and is required for male fertility and syncytial embryo development. Dev. Biol 334, 186–197. 10.1016/J.YDBIO.2009.07.016 [PubMed: 19631203]

Blatt P, Wong-Deyrup SW, McCarthy A, Breznak S, Hurton MD, Upadhyay M, Bennink B, Camacho J, Lee MT, Rangan P, 2021. RNA degradation is required for the germ-cell to maternal transition in Drosophila. Curr. Biol 31, 2984–2994.e7. 10.1016/j.cub.2021.04.052 [PubMed: 33989522]

Boley N, Wan KH, Bickel PJ, Celniker SE, 2014. Navigating and Mining modENCODE Data. Methods San Diego Calif 68, 38–47. 10.1016/j.ymeth.2014.03.007

Bowen ME, Attardi LD, 2019. The role of p53 in developmental syndromes. J. Mol. Cell Biol 11, 200–211. 10.1093/jmcb/mjy087 [PubMed: 30624728]

Buszczak M, Paterno S, Lighthouse D, Bachman J, Planck J, Owen S, Skora AD, Nystul TG, Ohlstein B, Allen A, Wilhelm JE, Murphy TD, Levis RW, Matunis E, Srivali N, Hoskins RA, Spradling AC, 2007. The Carnegie Protein Trap Library: A Versatile Tool for Drosophila Developmental Studies. Genetics 175, 1505–1531. 10.1534/genetics.106.065961 [PubMed: 17194782]

Calo E, Gu B, Bowen ME, Aryan F, Zalc A, Liang J, Flynn RA, Swigut T, Chang HY, Attardi LD, 2018. Tissue-selective effects of nucleolar stress and rDNA damage in developmental disorders. Nature 554, 112. [PubMed: 29364875]

Chen D, McKearin DM, 2003. A discrete transcriptional silencer in the bam gene determines asymmetric division of the Drosophila germline stem cell. Development 130, 1159–1170. 10.1242/dev.00325 [PubMed: 12571107]

Chen T, van Steensel B, 2017. Comprehensive analysis of nucleocytoplasmic dynamics of mRNA in Drosophila cells. PLOS Genet. 13, e1006929. 10.1371/journal.pgen.1006929 [PubMed: 28771467]

Chen Z-X, Sturgill D, Qu J, Jiang H, Park S, Boley N, Suzuki AM, Fletcher AR, Plachetzki DC, FitzGerald PC, Artieri CG, Atallah J, Barmina O, Brown JB, Blankenburg KP, Clough E, Dasgupta A, Gubbala S, Han Y, Jayaseelan JC, Kalra D, Kim Y-A, Kovar CL, Lee SL, Li M, Malley JD, Malone JH, Mathew T, Mattiuzzo NR, Munidasa M, Muzny DM, Ongeri F, Perales L, Przytycka TM, Pu L-L, Robinson G, Thornton RL, Saada N, Scherer SE, Smith HE, Vinson C, Warner CB, Worley KC, Wu Y-Q, Zou X, Cherbas P, Kellis M, Eisen MB, Piano F, Kionte K, Fitch DH, Sternberg PW, Cutter AD, Duff MO, Hoskins RA, Graveley BR, Gibbs RA, Bickel PJ, Kopp A, Carninci P, Celniker SE, Oliver B, Richards S, 2014. Comparative validation of the D. melanogaster modENCODE transcriptome annotation. Genome Res. 24, 1209–1223. 10.1101/gr.159384.113 [PubMed: 24985915]

Cheng Z, Mugler CF, Keskin A, Hodapp S, Chan LY-L, Weis K, Mertins P, Regev A, Jovanovic M, Brar GA, 2019. Small and Large Ribosomal Subunit Deficiencies Lead to Distinct Gene Expression Signatures that Reflect Cellular Growth Rate. Mol. Cell 73, 36–47.e10. 10.1016/j.molcel.2018.10.032 [PubMed: 30503772]

Corsini NS, Peer AM, Moeseneder P, Roiuk M, Burkard TR, Theussl H-C, Moll I, Knoblich JA, 2018. Coordinated Control of mRNA and rRNA Processing Controls Embryonic Stem Cell Pluripotency and Differentiation. Cell Stem Cell 22, 543–558.e12. 10.1016/j.stem.2018.03.002 [PubMed: 29625069]

De Cuevas M, Spradling AC, 1998. Morphogenesis of the Drosophila fusome and its implications for oocyte specification. Development 125, 2781 LP–2789. [PubMed: 9655801]

de la Cruz J, Karbstein K, Woolford JL, 2015. Functions of ribosomal proteins in assembly of eukaryotic ribosomes in vivo. Annu. Rev. Biochem 84, 93–129. 10.1146/annurev-biochem-060614-033917 [PubMed: 25706898]

Deisenroth C, Zhang Y, 2010. Ribosome biogenesis surveillance: Probing the ribosomal protein-Mdm2-p53 pathway. Oncogene 29, 4253–4260. 10.1038/onc.2010.189 [PubMed: 20498634]

DeLuca SZ, Spradling AC, 2018. Efficient Expression of Genes in the *Drosophila* Germline Using a UAS Promoter Free of Interference by Hsp70 piRNAs. Genetics 209, 381–387. 10.1534/genetics.118.300874 [PubMed: 29669732]

Flora P, Schowalter S, Wong-Deyrup S, DeGennaro M, Nasrallah MA, Rangan P, 2018a. Transient transcriptional silencing alters the cell cycle to promote germline stem cell differentiation in Drosophila. Dev. Biol 434, 84–95. 10.1016/j.ydbio.2017.11.014 [PubMed: 29198563]

Flora P, Wong-Deyrup SW, Martin ET, Palumbo RJ, Nasrallah M, Oligney A, Blatt P, Patel D, Fuchs G, Rangan P, 2018b. Sequential Regulation of Maternal mRNAs through a Conserved cis-Acting Element in Their 3' UTRs. Cell Rep 25, 3828–3843.e9. 10.1016/j.celrep.2018.12.007 [PubMed: 30590052]

Fonseca BD, Zakaria C, Jia J-J, Graber TE, Svitkin Y, Tahmasebi S, Healy D, Hoang H-D, Jensen JM, Diao IT, 2015. La-related protein 1 (LARP1) represses terminal oligopyrimidine (TOP) mRNA translation downstream of mTOR complex 1 (mTORC1). J. Biol. Chem 290, 15996–16020. [PubMed: 25940091]

Freed EF, Prieto J-L, McCann KL, McStay B, Baserga SJ, 2012. NOL11, Implicated in the Pathogenesis of North American Indian Childhood Cirrhosis, Is Required for Pre-rRNA Transcription and Processing. PLOS Genet. 8, e1002892. 10.1371/journal.pgen.1002892 [PubMed: 22916032]

Fuchs G, Diges C, Kohlstaedt LA, Wehner KA, Sarnow P, 2011. Proteomic Analysis of Ribosomes: Translational Control of mRNA populations by Glycogen Synthase GYS1. J. Mol. Biol 410, 118–130. 10.1016/j.jmb.2011.04.064 [PubMed: 21570405]

Gabut M, Bourdelais F, Durand S, 2020. Ribosome and Translational Control in Stem Cells. Cells 9, 497. 10.3390/cells9020497

Grandori C, Gomez-Roman N, Felton-Edkins ZA, Ngouenet C, Galloway DA, Eisenman RN, White RJ, 2005. c-Myc binds to human ribosomal DNA and stimulates transcription of rRNA genes by RNA polymerase I. Nat. Cell Biol 7, 311–318. 10.1038/ncb1224 [PubMed: 15723054]

Granneman S, Bernstein KA, Bleichert F, Baserga SJ, 2006. Comprehensive Mutational Analysis of Yeast DEXD/H Box RNA Helicases Required for Small Ribosomal Subunit Synthesis. Mol. Cell. Biol 26, 1183–1194. 10.1128/MCB.26.4.1183-1194.2006 [PubMed: 16449634]

Granneman S, Petfalski E, Tollervey D, Hurt EC, 2011. A cluster of ribosome synthesis factors regulate pre-rRNA folding and 5.8S rRNA maturation by the Rat1 exonuclease. EMBO J. 30, 4006–19. 10.1038/emboj.2011.256 [PubMed: 21811236]

Guillerez J, Lopez PJ, Proux F, Launay H, Dreyfus M, 2005. A mutation in T7 RNA polymerase that facilitates promoter clearance. Proc. Natl. Acad. Sci 102, 5958–5963. 10.1073/pnas.0407141102 [PubMed: 15831591]

Heinz S, Benner C, Spann N, Bertolino E, Lin YC, Laslo P, Cheng JX, Murre C, Singh H, Glass CK, 2010. Simple combinations of lineage-determining transcription factors prime cis-regulatory elements required for macrophage and B cell identities. Mol. Cell 38, 576–589. 10.1016/j.molcel.2010.05.004 [PubMed: 20513432]

Henras AK, Soudet J, Gérus M, Lebaron S, Caizergues-Ferrer M, Mougin A, Henry Y, 2008. The post-transcriptional steps of eukaryotic ribosome biogenesis. Cell. Mol. Life Sci 65, 2334–2359. 10.1007/s00018-008-8027-0 [PubMed: 18408888]

Higa-Nakamine S, Suzuki TT, Uechi T, Chakraborty A, Nakajima Y, Nakamura M, Hirano N, Suzuki TT, Kenmochi N, 2012. Loss of ribosomal RNA modification causes developmental defects in zebrafish. Nucleic Acids Res. 40, 391–398. 10.1093/nar/gkr700 [PubMed: 21908402]

Hinnant TD, Alvarez AA, Ables ET, 2017. Temporal remodeling of the cell cycle accompanies differentiation in the Drosophila germline. Dev. Biol 429, 118–131. 10.1016/j.ydbio.2017.07.001 [PubMed: 28711427]

Hong S, Freeberg MA, Han T, Kamath A, Yao Y, Fukuda T, Suzuki T, Kim JK, Inoki K, 2017. LARP1 functions as a molecular switch for mTORC1-mediated translation of an essential class of mRNAs. Elife 6, e25237. [PubMed: 28650797]

Hong S, Mannan AM, Inoki K, 2012. Evaluation of the Nutrient-Sensing mTOR Pathway, in: Weichhart T (Ed.), MTOR: Methods and Protocols, Methods in Molecular Biology. Humana Press, Totowa, NJ, pp. 29–44. 10.1007/978-1-61779-430-8_3

Hornstein E, Tang H, Meyuhas O, 2001. Mitogenic and nutritional signals are transduced into translational efficiency of TOP mRNAs, in: Cold Spring Harbor Symposia on Quantitative Biology. Cold Spring Harbor Laboratory Press, pp. 477–484.

Hsu H-J, LaFever L, Drummond-Barbosa D, 2008. Diet controls normal and tumorous germline stem cells via insulin-dependent and -independent mechanisms in Drosophila. Dev. Biol 313, 700–712. 10.1016/j.ydbio.2007.11.006 [PubMed: 18068153]

Hu Y, Flockhart I, Vinayagam A, Bergwitz C, Berger B, Perrimon N, Mohr SE, 2011. An integrative approach to ortholog prediction for disease-focused and other functional studies. BMC Bioinformatics 12, 357. 10.1186/1471-2105-12-357 [PubMed: 21880147]

Iadevaia V, Liu R, Proud CG, 2014. mTORC1 signaling controls multiple steps in ribosome biogenesis. Semin. Cell Dev. Biol., Development of the urogenital system & mTOR Signalling & Tight Junctions in Health and Disease 36, 113–120. 10.1016/j.semcdb.2014.08.004

Ichihara K, Shimizu H, Taguchi O, Yamaguchi M, Inoue YH, 2007. A Drosophila orthologue of larp protein family is required for multiple processes in male meiosis. Cell Struct. Funct 710190003.

Jefferies HBJ, Fumagalli S, Dennis PB, Reinhard C, Pearson RB, Thomas G, 1997. Rapamycin suppresses 5′TOP mRNA translation through inhibition of p70s6k. EMBO J. 16, 3693–3704. 10.1093/emboj/16.12.3693 [PubMed: 9218810]

Jia J-J, Lahr RM, Solgaard MT, Moraes BJ, Pointet R, Yang A-D, Celucci G, Graber TE, Hoang H-D, Niklaus MR, Pena IA, Hollensen AK, Smith EM, Chaker-Margot M, Anton L, Dajadian C, Livingstone M, Hearnden J, Wang X-D, Yu Y, Maier T, Damgaard CK, Berman AJ, Alain T, Fonseca BD, 2021. mTORC1 promotes TOP mRNA translation through site-specific phosphorylation of LARP1. Nucleic Acids Res. 10.1093/nar/gkaa1239

Jones NC, Lynn ML, Gaudenz K, Sakai D, Aoto K, Rey J-P, Glynn EF, Ellington L, Du C, Dixon J, Dixon MJ, Trainor PA, 2008. Prevention of the neurocristopathy Treacher Collins syndrome through inhibition of p53 function. Nat. Med 14, 125–133. 10.1038/nm1725 [PubMed: 18246078]

Kai T, Spradling A, 2003. An empty Drosophila stem cell niche reactivates the proliferation of ectopic cells.

Karpen GH, Schaefer JE, Laird CD, 1988. A Drosophila rRNA gene located in euchromatin is active in transcription and nucleolus formation. Genes Dev. 2, 1745–1763. [PubMed: 3149250]

Khajuria RK, Munschauer M, Ulirsch JC, Fiorini C, Ludwig LS, McFarland SK, Abdulhay NJ, Specht H, Keshishian H, Mani DRR, Jovanovic M, Ellis SR, Fulco CP, Engreitz JM, Schütz S, Lian J, Gripp KW, Weinberg OK, Pinkus GS, Gehrke L, Regev A, Lander ES, Gazda HT, Lee WY, Panse VG, Carr SA, Sankaran VG, 2018. Ribosome levels selectively regulate translation and lineage commitment in human hematopoiesis. Cell 173, 90–103. 10.1016/J.CELL.2018.02.036 [PubMed: 29551269]

Kimball SR, 2002. Regulation of Global and Specific mRNA Translation by Amino Acids. J. Nutr 132, 883–886. 10.1093/jn/132.5.883 [PubMed: 11983807]

Koš M, Tollervey D, 2010. Yeast pre-rRNA processing and modification occur cotranscriptionally. Mol. Cell 37, 809–820. [PubMed: 20347423]

Lahr RM, Fonseca BD, Ciotti GE, Al-Ashtal HA, Jia J-J, Niklaus MR, Blagden SP, Alain T, Berman AJ, 2017. La-related protein 1 (LARP1) binds the mRNA cap, blocking eIF4F assembly on TOP mRNAs. Elife 6, e24146. [PubMed: 28379136]

Lahr RM, Mack SM, Héroux A, Blagden SP, Bousquet-Antonelli C, Deragon J-M, Berman AJ, 2015. The La-related protein 1-specific domain repurposes HEAT-like repeats to directly bind a 5′TOP sequence. Nucleic Acids Res. 43, 8077–8088. 10.1093/nar/gkv748 [PubMed: 26206669]

Li L, Pang X, Zhu Z, Lu L, Yang J, Cao J, Fei S, 2018. GTPBP4 Promotes Gastric Cancer Progression via Regulating P53 Activity. Cell. Physiol. Biochem 45, 667–676. [PubMed: 29408813]

Lipton JM, Kudisch M, Gross R, Nathan DG, 1986. Defective Erythroid Progenitor Differentiation System in Congenital Hypoplastic (Diamond-Blackfan) Anemia. Blood 67, 962–968. 10.1182/blood.V67.4.962.962 [PubMed: 3955239]

Loewith R, Hall MN, 2011. Target of Rapamycin (TOR) in Nutrient Signaling and Growth Control. Genetics 189, 1177–1201. 10.1534/genetics.111.133363 [PubMed: 22174183]

Lu W-J, Chapo J, Roig I, Abrams JM, 2010. Meiotic Recombination Provokes Functional Activation of the p53 Regulatory Network. Science 328, 1278–1281. 10.1126/science.1185640

Lunardi A, Di Minin G, Provero P, Dal Ferro M, Carotti M, Del Sal G, Collavin L, 2010. A genome-scale protein interaction profile of Drosophila p53 uncovers additional nodes of the human p53 network. Proc. Natl. Acad. Sci 107, 6322–6327. [PubMed: 20308539]

Mathieu J, Cauvin C, Moch C, Radford SJJ, Sampaio P, Perdigoto CN, Schweisguth F, Bardin AJ, Sunkel CE, McKim K, Echard A, Huynh J-R, 2013. Aurora B and cyclin B have opposite effects on the timing of cytokinesis abscission in Drosophila germ cells and in vertebrate somatic cells. Dev. Cell 26, 250–265. 10.1016/J.DEVCEL.2013.07.005 [PubMed: 23948252]

Matias NR, Mathieu J, Huynh J-R, 2015. Abscission is regulated by the ESCRT-III protein shrub in Drosophila germline stem cells. PLoS Genet. 11, e1004653. 10.1371/journal.pgen.1004653 [PubMed: 25647097]

McCarthy A, Deiulio A, Martin ET, Upadhyay M, Rangan P, 2018. Tip60 complex promotes expression of a differentiation factor to regulate germline differentiation in female Drosophila. Mol. Biol. Cell 29, 2933–2945. 10.1091/mbc.E18-06-0385 [PubMed: 30230973]

McCarthy A, Sarkar K, Martin ET, Upadhyay M, James JR, Lin JM, Jang S, Williams ND, Forni PE, Buszczak M, Rangan P, 2019. MSL3 coordinates a transcriptional and translational meiotic program in female Drosophila. bioRxiv 2019.12.18.879874. 10.1101/2019.12.18.879874

McKearin D, Ohlstein B, 1995. A role for the Drosophila bag-of-marbles protein in the differentiation of cystoblasts from germline stem cells. Development 121, 2937 LP–2947. [PubMed: 7555720]

Meyuhas O, 2000. Synthesis of the translational apparatus is regulated at the translational level. Eur. J. Biochem 267, 6321–6330. 10.1046/j.1432-1327.2000.01719.x [PubMed: 11029573]

Meyuhas O, Kahan T, 2015. The race to decipher the top secrets of TOP mRNAs. Biochim. Biophys. Acta BBA - Gene Regul. Mech 1849, 801–811. 10.1016/j.bbagrm.2014.08.015

Mills EW, Green R, 2017. Ribosomopathies: There's strength in numbers. Science 358, eaan2755. 10.1126/SCIENCE.AAN2755 [PubMed: 29097519]

Moon S, Cassani M, Lin YA, Wang L, Dou K, Zhang ZZZ, 2018. A Robust Transposon-Endogenizing Response from Germline Stem Cells. Dev. Cell 47, 660–671. [PubMed: 30393075]

Nerurkar P, Altvater M, Gerhardy S, Schütz S, Fischer U, Weirich C, Panse VG, 2015. Eukaryotic ribosome assembly and nuclear export. Int. Rev. Cell Mol. Biol 319, 107–40. 10.1016/bs.ircmb.2015.07.002

O 'day CL, Chavanikamannil F, Abelson J, 1996. 8S rRNA processing requires the RNA helicase-like protein Rrp3. Nucleic Acids Res. 24.

Ochs RL, Lischwe MA, Spohn WH, Busch H, 1985. Fibrillarin: a new protein of the nucleolus identified by autoimmune sera. Biol. Cell 54, 123–133. 10.1111/j.1768-322X.1985.tb00387.x [PubMed: 2933102]

Ohlstein B, McKearin D, 1997. Ectopic expression of the Drosophila Bam protein eliminates oogenic germline stem cells. Development 124, 3651–3662. [PubMed: 9342057]

Pagès H, Aboyoun P, Gentleman R, DebRoy S, 2019. Biostrings: Efficient manipulation of biological strings.

Panov KI, Hannan K, Hannan RD, Hein N, 2021. The Ribosomal Gene Loci—The Power behind the Throne. Genes 12. 10.3390/genes12050763

Pereboom TC, van Weele LJ, Bondt A, MacInnes AW, 2011. A zebrafish model of dyskeratosis congenita reveals hematopoietic stem cell formation failure resulting from ribosomal protein-mediated p53 stabilization. Blood 118, 5458–5465. [PubMed: 21921046]

Philippe L, van den Elzen AMG, Watson MJ, Thoreen CC, 2020. Global analysis of LARP1 translation targets reveals tunable and dynamic features of 5′ TOP motifs. Proc. Natl. Acad. Sci 117, 5319–5328. 10.1073/pnas.1912864117 [PubMed: 32094190]

Philippe L, Vasseur J-J, Debart F, Thoreen CC, 2018. La-related protein 1 (LARP1) repression of TOP mRNA translation is mediated through its cap-binding domain and controlled by an adjacent regulatory region. Nucleic Acids Res. 46, 1457–1469. 10.1093/nar/gkx1237 [PubMed: 29244122]

Qin X, Ahn S, Speed TP, Rubin GM, 2007. Global analyses of mRNA translational control during early Drosophila embryogenesis. Genome Biol. 8, R63. 10.1186/gb-2007-8-4-r63 [PubMed: 17448252]

Rørth P, 1998. Gal4 in the Drosophila female germline. Mech. Dev 78, 113–118. 10.1016/S0925-4773(98)00157-9 [PubMed: 9858703]

Sanchez CG, Teixeira FK, Czech B, Preall JB, Zamparini AL, Seifert JRK, Malone CD, Hannon GJ, Lehmann R, 2016. Regulation of Ribosome Biogenesis and Protein Synthesis Controls Germline Stem Cell Differentiation. Cell Stem Cell 18, 276–290. 10.1016/J.STEM.2015.11.004 [PubMed: 26669894]

Sarov M, Barz C, Jambor H, Hein MY, Schmied C, Suchold D, Stender B, Janosch S, KJ VV, Krishnan R, Krishnamoorthy A, Ferreira IR, Ejsmont RK, Finkl K, Hasse S, Kämpfer P, Plewka N, Vinis E, Schloissnig S, Knust E, Hartenstein V, Mann M, Ramaswami M, VijayRaghavan K, Tomancak P, Schnorrer F, 2016. A genome-wide resource for the analysis of protein localisation in Drosophila. eLife 5, e12068. 10.7554/eLife.12068 [PubMed: 26896675]

Sekiguchi T, Hayano T, Yanagida M, Takahashi N, Nishimoto T, 2006. NOP132 is required for proper nucleolus localization of DEAD-box RNA helicase DDX47. Nucleic Acids Res. 34, 4593–4608. 10.1093/nar/gkl603 [PubMed: 16963496]

Senturk E, Manfredi JJ, 2013. p53 and Cell Cycle Effects After DNA Damage. Methods Mol. Biol Clifton NJ 962, 49–61. 10.1007/978-1-62703-236-0_4 [PubMed: 23150436]

Serano TL, Cheung H-K, Frank LH, Cohen RS, 1994. P element transformation vectors for studying Drosophila melanogaster oogenesis and early embryogenesis. Gene 138, 181–186. 10.1016/0378-1119(94)90804-4 [PubMed: 8125300]

Sezgin M, Sankur B, 2004. Survey over image thresholding techniques and quantitative performance evaluation. J. Electron. Imaging 13, 146–166.

Sloan KE, Warda AS, Sharma S, Entian KD, Lafontaine DLJ, Bohnsack MT, 2017. Tuning the ribosome: The influence of rRNA modification on eukaryotic ribosome biogenesis and function. RNA Biol. 14, 1138–1152. 10.1080/15476286.2016.1259781 [PubMed: 27911188]

Studier FW, 2005. Protein production by auto-induction in high-density shaking cultures. Protein Expr. Purif 41, 207–234. 10.1016/j.pep.2005.01.016 [PubMed: 15915565]

Tafforeau L, Zorbas C, Langhendries J-L, Mullineux S-T, Stamatopoulou V, Mullier R, Wacheul L, Lafontaine DLJ, 2013. The Complexity of Human Ribosome Biogenesis Revealed by Systematic Nucleolar Screening of Pre-rRNA Processing Factors. Mol. Cell 51, 539–551. 10.1016/J.MOLCEL.2013.08.011 [PubMed: 23973377]

Tang H, Hornstein E, Stolovich M, Levy G, Livingstone M, Templeton D, Avruch J, Meyuhas O, 2001. Amino Acid-Induced Translation of TOP mRNAs Is Fully Dependent on Phosphatidylinositol 3-Kinase-Mediated Signaling, Is Partially Inhibited by Rapamycin, and Is Independent of S6K1 and rpS6 Phosphorylation. Mol. Cell. Biol 21, 8671–8683. 10.1128/MCB.21.24.8671-8683.2001 [PubMed: 11713299]

Thomas PD, Campbell MJ, Kejariwal A, Mi H, Karlak B, Daverman R, Diemer K, Muruganujan A, Narechania A, 2003. PANTHER: A Library of Protein Families and Subfamilies Indexed by Function. Genome Res. 13, 2129–2141. 10.1101/gr.772403 [PubMed: 12952881]

Thoreen CC, Chantranupong L, Keys HR, Wang T, Gray NS, Sabatini DM, 2012. A unifying model for mTORC1-mediated regulation of mRNA translation. Nature 485, 109–113. 10.1038/nature11083 [PubMed: 22552098]

Tye BW, Commins N, Ryazanova LV, Wühr M, Springer M, Pincus D, Churchman LS, 2019. Proteotoxicity from aberrant ribosome biogenesis compromises cell fitness. eLife 8, e43002. 10.7554/eLife.43002 [PubMed: 30843788]

Upadhyay M, Cortez YM, Wong-Deyrup S, Tavares L, Schowalter S, Flora P, Hill C, Nasrallah MA, Chittur S, Rangan P, 2016. Transposon Dysregulation Modulates dWnt4 Signaling to Control Germline Stem Cell Differentiation in Drosophila. PLOS Genet. 12, e1005918. 10.1371/journal.pgen.1005918 [PubMed: 27019121]

Venema J, Cile Bousquet-Antonelli C, Gelugne J-P, Le Caizergues-Ferrer M, Tollervey D, 1997. Rok1p Is a Putative RNA Helicase Required for rRNA Processing 17, 3398–3407.

Vincent NG, Charette JM, Baserga SJ, 2017. The SSU processome interactome in Saccharomyces cerevisiae reveals potential new protein subcomplexes. RNA rna.062927.117. 10.1261/rna.062927.117

Watkins NJ, Bohnsack MT, 2012. The box C/D and H/ACA snoRNPs: Key players in the modification, processing and the dynamic folding of ribosomal RNA. Wiley Interdiscip. Rev. RNA 3, 397–414. 10.1002/wrna.117 [PubMed: 22065625]

Wei Y, Bettedi L, Kim K, Ting C-Y, Lilly M, 2019. The GATOR complex regulates an essential response to meiotic double-stranded breaks in Drosophila. eLife 8, e42149. 10.7554/eLife.42149 [PubMed: 31650955]

Wei Y, Reveal B, Reich J, Laursen WJ, Senger S, Akbar T, Iida-Jones T, Cai W, Jarnik M, Lilly MA, 2014. TORC1 regulators Iml1/GATOR1 and GATOR2 control meiotic entry and oocyte development in Drosophila. Proc. Natl. Acad. Sci 111, E5670–E5677. [PubMed: 25512509]

Woolnough JL, Atwood BL, Liu Z, Zhao R, Giles KE, 2016. The Regulation of rRNA Gene Transcription during Directed Differentiation of Human Embryonic Stem Cells. PLOS ONE 11, e0157276. 10.1371/journal.pone.0157276 [PubMed: 27299313]

Xie T, Spradling AC, 2000. A Niche Maintaining Germ Line Stem Cells in the Drosophila Ovary. Science 290, 328–330. 10.1126/science.290.5490.328 [PubMed: 11030649]

Xie T, Spradling AC, 1998. decapentaplegic Is Essential for the Maintenance and Division of Germline Stem Cells in the Drosophila Ovary. Cell 94, 251–260. 10.1016/S0092-8674(00)81424-5 [PubMed: 9695953]

Zhang Q, Shalaby NA, Buszczak M, 2014. Changes in rRNA transcription influence proliferation and cell fate within a stem cell lineage. Science 343, 298–301. [PubMed: 24436420]

Zhang Y, Forys JT, Miceli AP, Gwinn AS, Weber JD, 2011. Identification of DHX33 as a Mediator of rRNA Synthesis and Cell Growth. Mol. Cell. Biol 31, 4676–4691. 10.1128/MCB.05832-11 [PubMed: 21930779]

Zhou R, Mohr S, Hannon GJ, Perrimon N, 2013. Inducing RNAi in Drosophila Cells by Transfection with dsRNA. Cold Spring Harb. Protoc 2013, pdb.prot074351-pdb.prot074351. 10.1101/pdb.prot074351

Zielke N, Korzelius J, van Straaten M, Bender K, Schuhknecht GFP, Dutta D, Xiang J, Edgar BA, 2014. Fly-FUCCI: A versatile tool for studying cell proliferation in complex tissues. Cell Rep. 7, 588–598. [PubMed: 24726363]

**Highlights:**

- Ais, Ath, and Pths are required for efficient RiBi in *Drosophila*
- RiBi defects leads to repression of TOP-containing mRNAs
- Larp regulates TOP-containing mRNAs to balance RiBi
- Efficient RiBi is required for translation of Non1, a p53 regulator

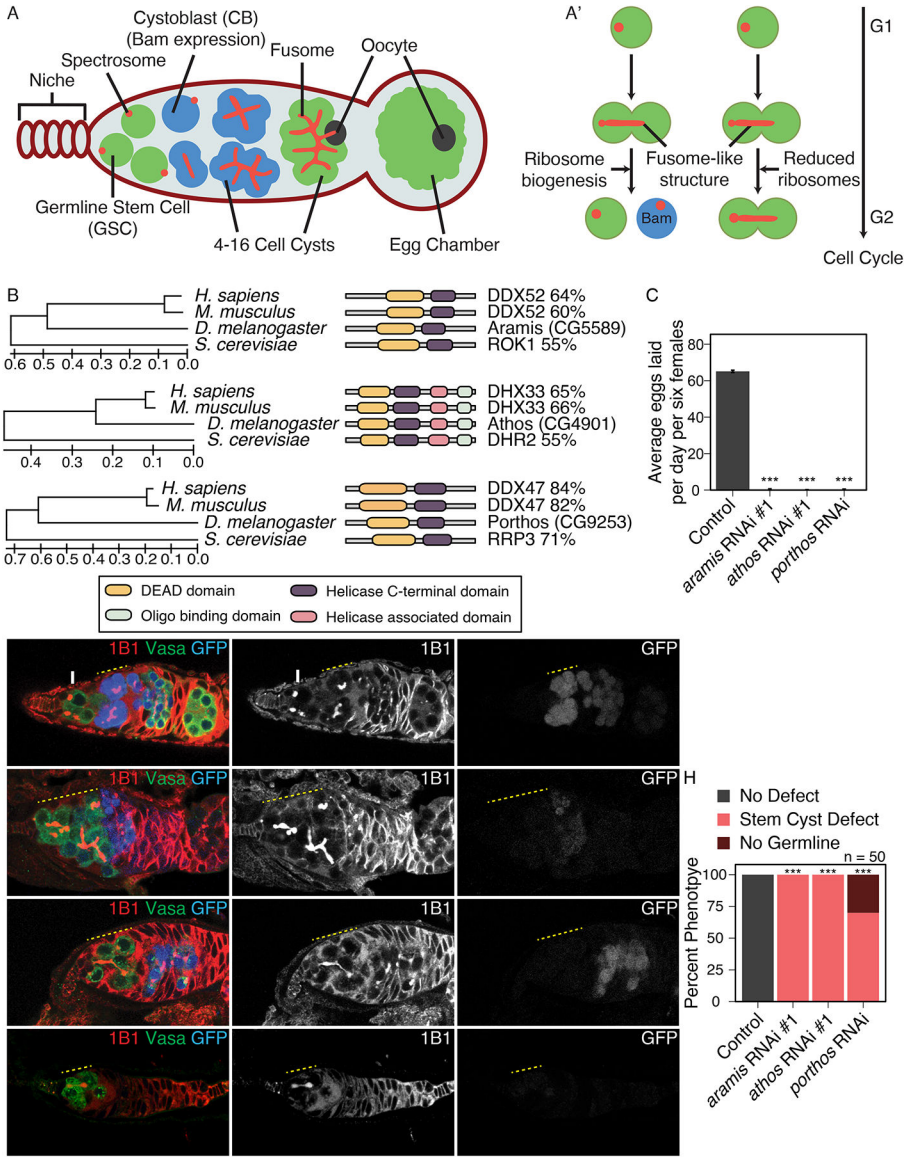


**Figure 1: DExD/H-box proteins Ais, Ath and Pths are required for GSC differentiation.**

(**A**) Schematic of *Drosophila* germarium. (**A'**) RiBi promotes GSC cytokinesis and differentiation. (**B**) Conservation of *ais*, *ath*, and *pths* between *H. sapiens*, *D. melanogaster*, and *S. cerevisiae* (left). Representation of conserved protein domains for DExD/H-box proteins in *Drosophila* compared to *H. sapiens* and *S. cerevisiae* orthologs (right). Percentage values represent similarity to *Drosophila* orthologs. (**C**) Fertility of *ais*, *ath* or *pths* GKD compared to *nosGAL4* (n=3 trials). ***=p<0.001, Tukey's post-hoc test after one-way ANOVA, p<0.001. Data are mean±standard error (SE). (**D-G"**) Images of ovaries from control (**D-D"**) and (**E-E"**) *ais*, (**F-F"**) *ath* or (**G-G"**) *pths* GKD stained for 1B1 (red, left grayscale), Vasa (green), and Bam-GFP (blue, right grayscale). GKD of these genes (**E-G"**) results in germ cells marked by a 1B1 positive, fusome-like structure (yellow line) in contrast to the single cells present in (**D-D"**) controls (white arrow) or Bam expressing differentiating cysts (yellow line). (**H**) Phenotype quantification of ovaries depleted of *ais*,

*ath* or *pths* compared to control ovaries (n=50 ovarioles, df=2, ***=p<0.001, Fisher's exact tests with Holm correction). Data are percent. Scale bars are 15 μm.

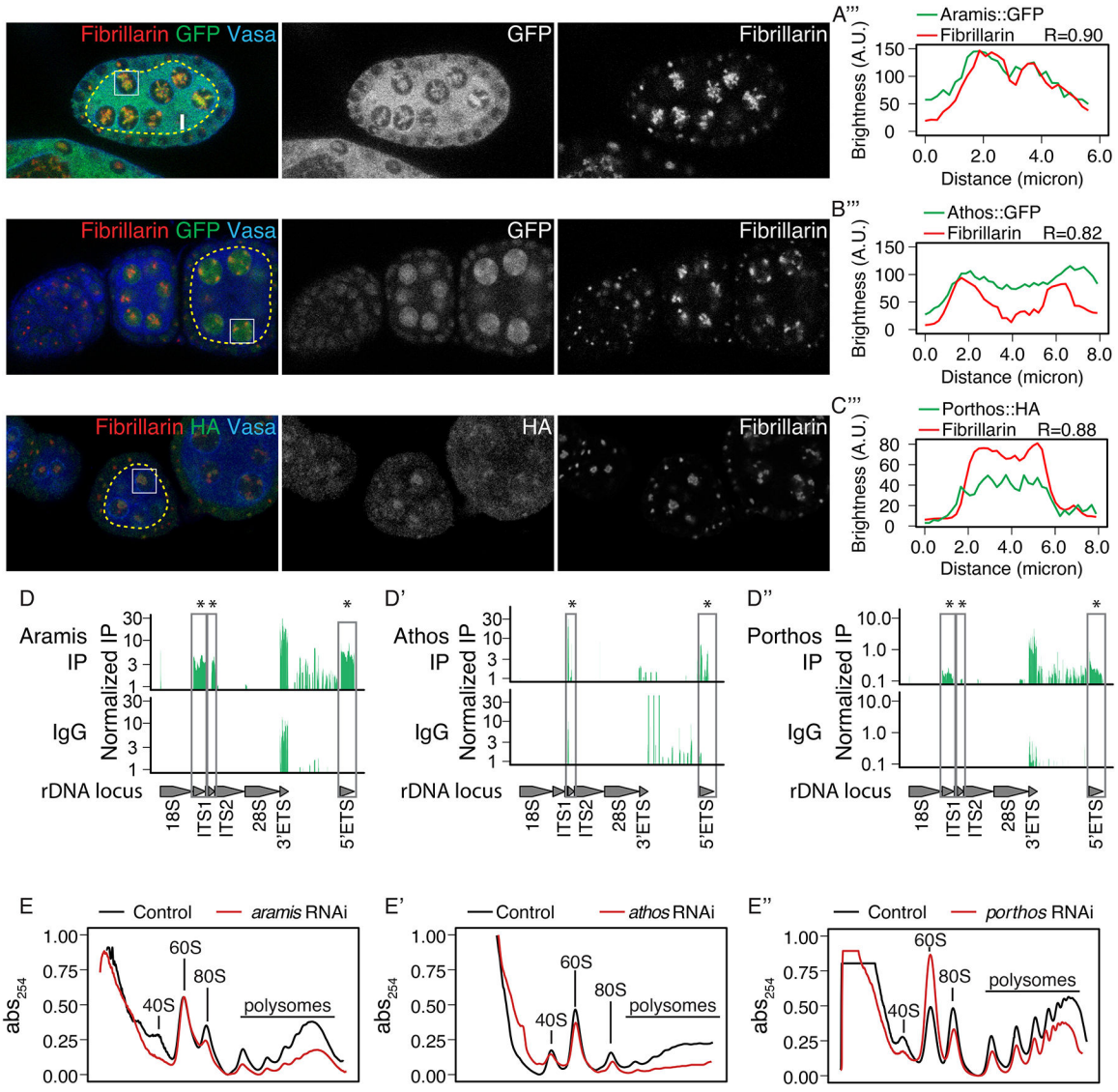


**Figure 2. Ais, Ath, and Pths are required for efficient RiBi.**

(**A-C”**) Images of an ovariole stained for Fibrillarin (red, right grayscale), Vasa (blue), (**A-A”**) Ais::GFP, (**B-B”**) Ath::GFP and (**C-C”**) Pths::HA (green, left grayscale). (**A”’-C”’**) Fluorescence intensity plot of stainings. The white box indicates the quantified nucleus, while the yellow outline indicates the germline. R values denote Spearman correlation coefficients between GFP and Fibrillarin. (**D-D”**) RNA IP-seq of (**D**) Ais, (**D’**) Ath, and (**D”**) Pths aligned to an rDNA locus. Bar height represents log scaled rRNA reads mapping to rDNA normalized to input and spike-in. Grey boxes outline ETS (external spacers) and ITS (internal spacers) which are only present in pre-rRNA that are significantly enriched in the IP compared to the IgG control (bootstrapped paired t-tests, n=3, *=p<0.05). (**E-E”**) Polysome traces from S2 cells treated with dsRNA targeting (**E**) *ais*, (**E’**) *ath*, (**E”**) *pths* (red line) compared to a mock transfection control (black line). *ais*, ath and pths are required to maintain a proper 40S/60S ribosomal subunit ratio and polysome levels compared to control. Scale bars are 15 μm.

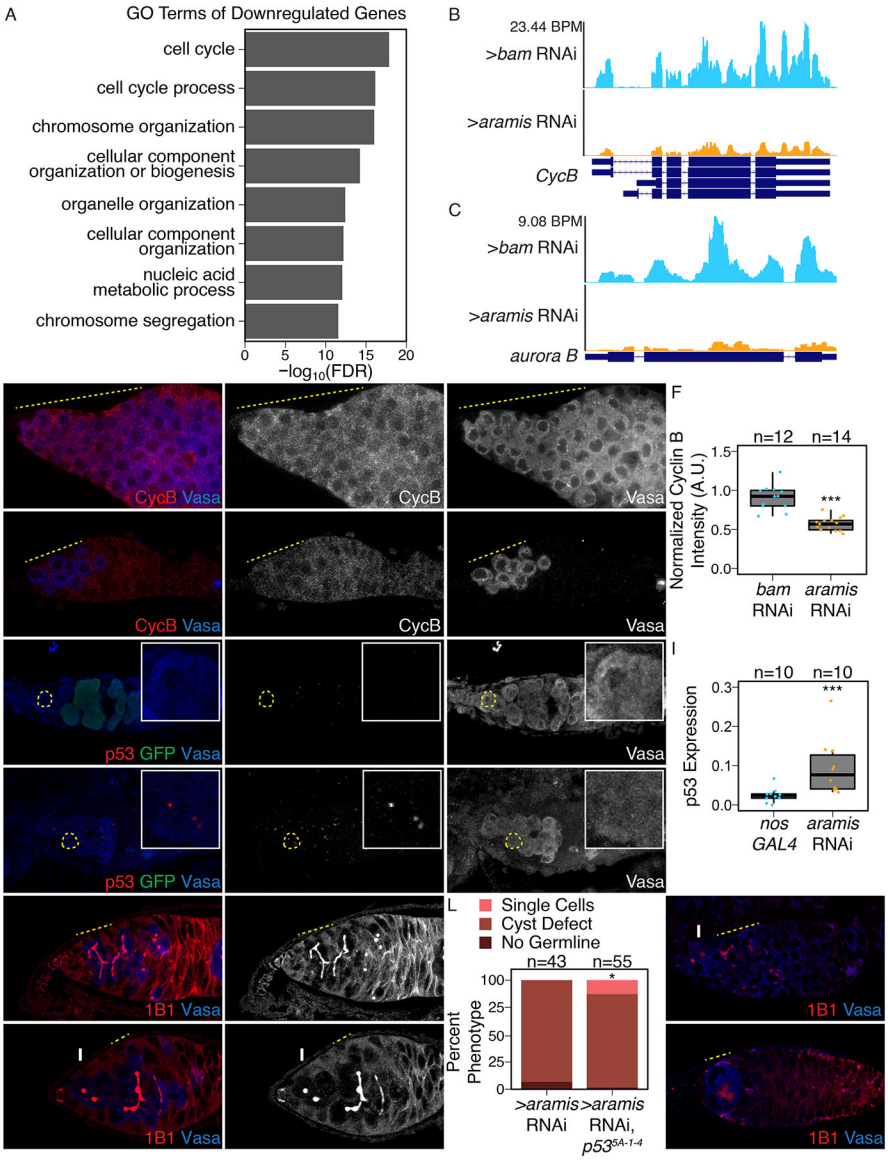


**Figure 3. Ais, Ath, and Pths are required for cell cycle progression.**

(**A**) Plot of the significant Biological Process GO-terms of downregulated genes from *ais* GKD compared to *bam* GKD control. (**B-C**) Genome browser tracks showing the locus of (**B**) *CycB* and (**C**) a*urora B* in *ais* GKD ovaries compared to *bam* GKD. Y-axis represents bases per million (BPM). (**D-E”**) Images of germaria stained for CycB (red, left grayscale) and Vasa (blue, right grayscale) in (**D-D”’**) *bam* GKD control ovaries and (**E-E”**) *ais* GKD. (**F**) Boxplot of CycB intensity in the germline normalized to CycB intensity in the soma in *bam* GKD and *ais* GKD (n=12–14 germaria per sample, ***=p<0.001, Welch t-test. (**G-H”**) Images of germaria stained for p53 (red, left grayscale), GFP (green), and Vasa (blue, right grayscale) in (**G-G”**) *nosGAL4* ovaries and (**H-H”**) *ais* GKD. Cells in yellow circle represent cells in the insets. (**I**) Box plot of percentage of pixel area exceeding the background threshold for p53 in GSCs and CBs in control and *ais* GKD indicates p53 expression is elevated in GSCs/CBs of *ais* GKD. (n=10 germaria per sample, ***=p<0.001,

Welch's t-test. (**J-K"**) Images of germaria stained for 1B1 (red, left grayscale) and Vasa (blue, right grayscale) in (**J-J"**) *ais* GKD and (**K-K"**) *ais* GKD in a $p53^{5\text{-}A\text{-}14}$ background. (**L**) Quantification of stem-cyst phenotypes in *ais* GKD compared to the $p53^{5\text{-}A\text{-}14}$, *ais* GKD (n=43–55 germaria per genotype, df=2, Fisher's exact test $p< 0.05$). (**M-N**) Images of ovaries stained for 1B1 (red) and Vasa (blue) in *nosGAL4* ovaries (**M**) and (**N**) *p53* OE in the germline. Cysts are denoted by a yellow line, single cells by a white arrow. 84% of germaria from *p53* OE ovaries lost germline while 12% contained a cyst and 4% accumulated single cells (n=55 germaria, Fisher's exact test, $p<0.001$). Scale bar for main images is 15 μm, scale bar for insets is 3.75 μm.

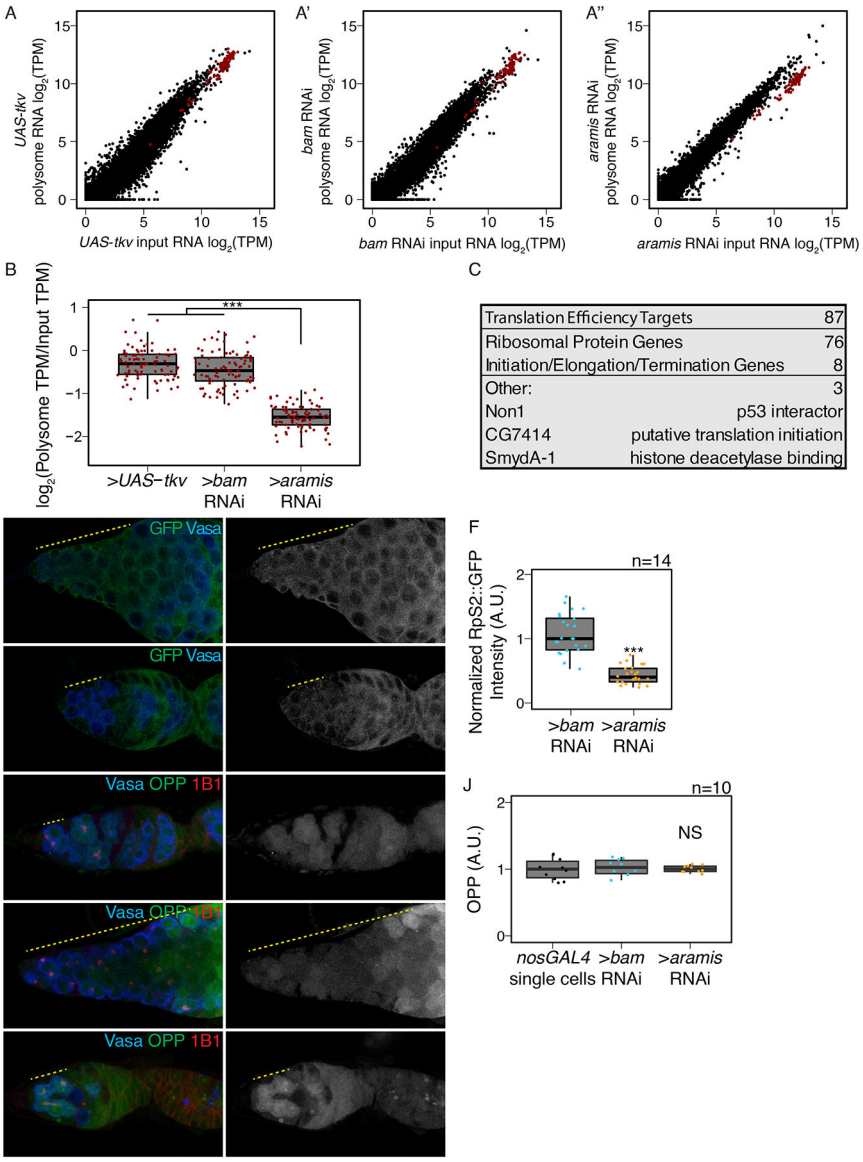


**Figure 4. Ais is required for efficient translation of a subset of mRNAs.**

(**A-A”**) Biplots of mRNA input versus polysome associated mRNA from ovaries enriched for (**A**) GSCs (*UAS-tkv*), (**A’**) CBs (*bam* GKD) or (**A”**) *ais* GKD ovaries. (**B**) Boxplot of translation efficiency of target genes in *UAS-tkv*, *bam* GKD and *ais* GKD samples (ANOVA p<0.001, post-hoc Welch’s t-test, n=87, ***=p<0.001). (**C**) Summary of downregulated target genes. (**D-E’**) Images of germaria stained for 1B1 (red), RpS2::GFP (green, grayscale), and Vasa (blue) in (**D-D’**) *bam* GKD control and (**E-E’**) *ais* GKD (yellow line marks approximate region of germline used for quantification). (**F**) Quantification of germline RpS2::GFP expression, normalized to RpS2::GFP expression in the soma, in *bam* GKD compared to *ais* GKD (n=14 germaria per sample, Welch’s t-test, ***=p<0.001). (**G-I’**) Images of germaria stained for 1B1 (red), OPP (green, grayscale), and Vasa (blue) in (**G-G’**) *nosGAL4*, (**H-H’**) *bam* GKD, and (**I-I’**) *ais* GKD (yellow line marks approximate region of germline used for quantification). (**J**) Quantification of OPP in single cells of

control germaria and CBs in *bam* GKD as controls and *ais* GKD (n = 10 germaria per genotype, Welch's t-test, NS = p>0.05). Scale bars are 15 μm.

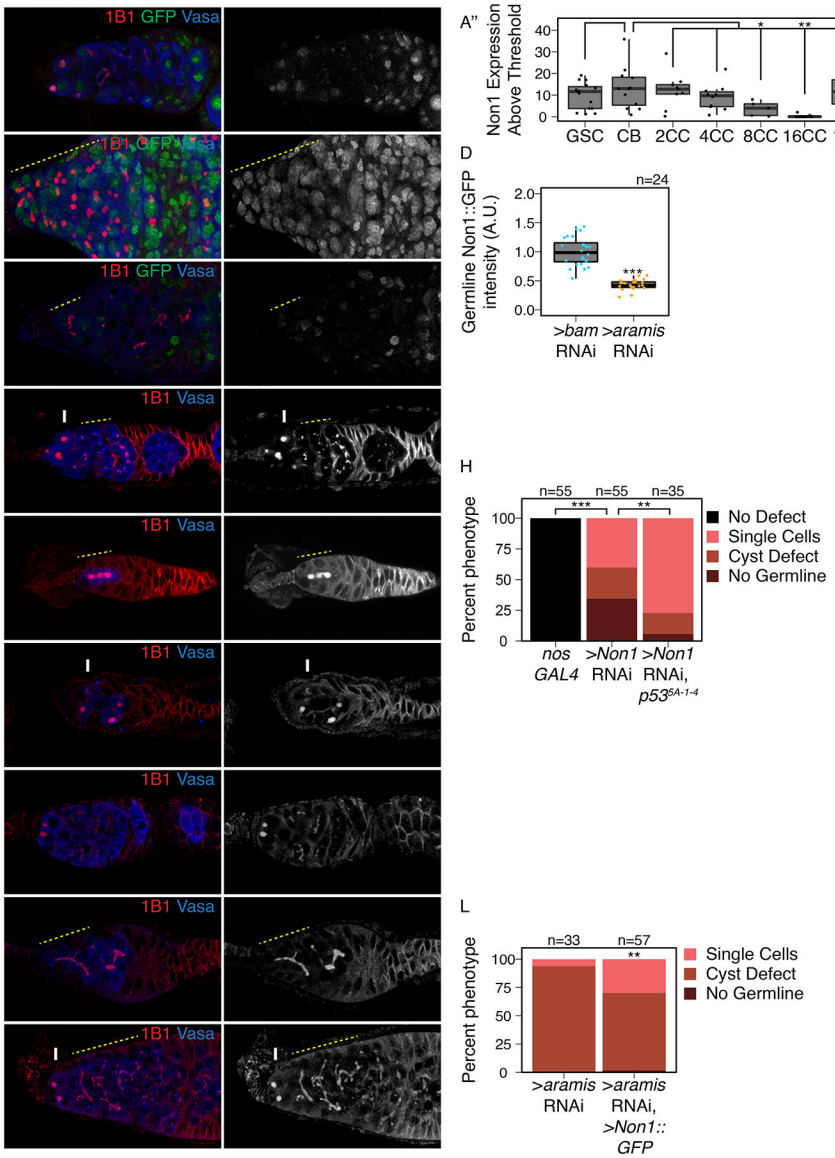


**Figure 5. Non1 represses p53 expression to allow for GSC differentiation.**

(**A-A'**) Non1::GFP germaria stained for 1B1 (red), GFP (green, grayscale), and Vasa (blue). (**A"**) Boxplot of Non1::GFP expression over germline development (n=5–25 cysts of each type, *=p<0.05, **=p<0.01, ANOVA with Welch's post-hoc tests). (**B-C'**) Images of (**B-B'**) *bam* GKD and (**C-C'**) *ais* GKD germaria expressing *Non1::GFP*, stained for 1B1 (red), Vasa (blue), and Non1::GFP (green, grayscale). Yellow line marks region of germline used for quantification. (**D**) Boxplot of Non1::GFP expression in the germline normalized to somatic Non1::GFP expression in *bam* GKD and *ais* GKD (n=24 germaria per genotype, Welch's t-test, ***=p<0.001). (**E-G'**) Images of germaria stained for 1B1 (red, grayscale) and Vasa (blue) in (**E-E'**) *nosGAL4* control ovaries, (**F-F'**) *Non1* GKD, and (**G-G'**) *Non1* GKD in a $p53^{5\text{-}A\text{-}1\text{-}4}$ background. Arrow marks a single cell (**E, G**), yellow line marks a stem-cyst (**F-F'**) or the presence of cysts (**E-E'**). (**H**) Percentage of germaria with no defect (black), single cells (salmon), stem-cyst proximal to the niche (brown-red), or germline loss

(dark red) demonstrates a significant rescue of stem-cyst formation upon of loss of *Non1* in $p53^{5\text{-}A\text{-}14}$ compared to the *p53* control (n=35–55 germaria per genotype, df=3, Fisher's exact test with Holm correction **=p< 0.01, ***=p< 0.001). (**I-K'**) Images of germaria stained for 1B1 (red, grayscale) and Vasa (blue) in ovaries with (**I-I'**) germline Non1 OE, (**J-J'**) *ais* GKD and (**K-K**') *ais* GKD with *Non1* OE results in more single cells (white arrow). (**L**) Phenotypic quantification of *ais* GKD with *Non1* OE (n=33–57 germaria per genotype, df=2, Fisher's exact test, **=p< 0.01). Scale bars are 15 μm.

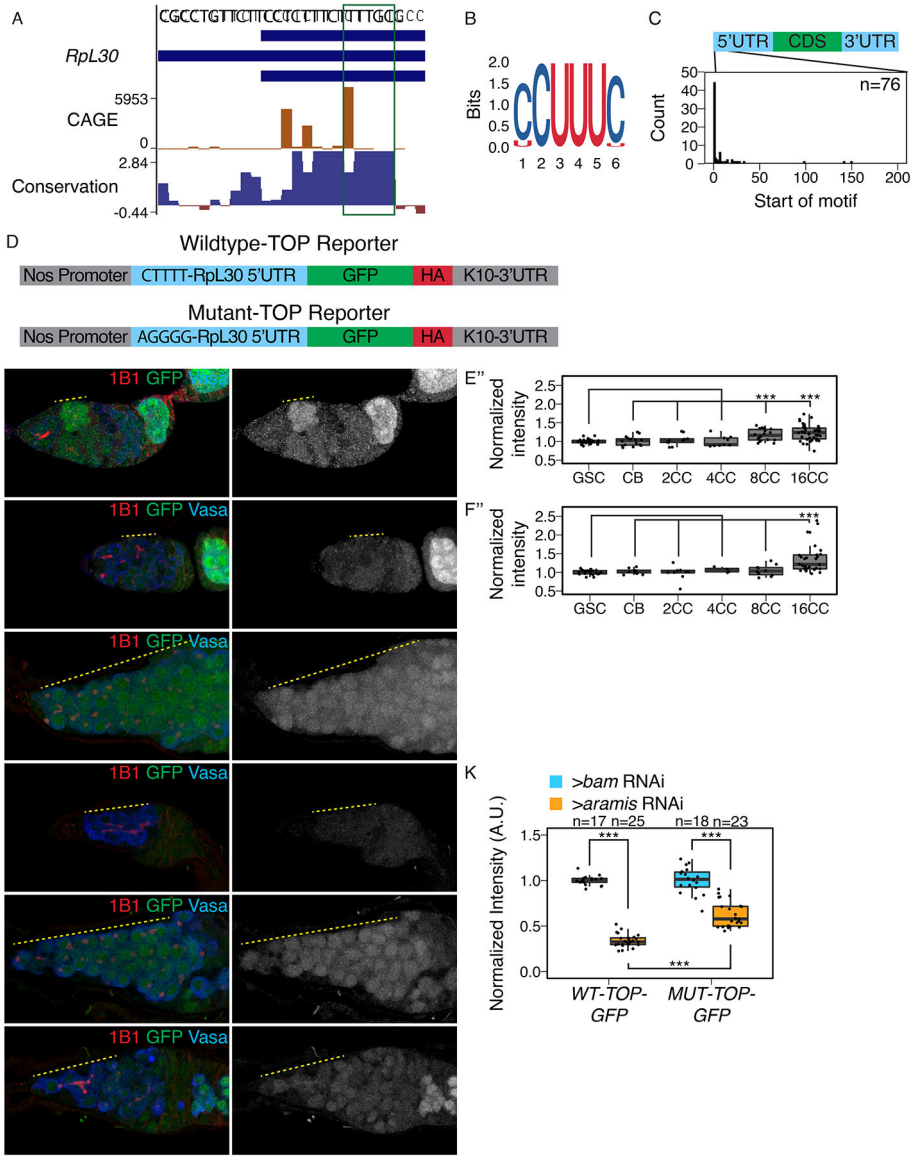


**Figure 6. Ais regulated mRNAs contain a TOP motif.**

(**A**) *RpL30* locus from CAGE-seq data showing TSSs (orange) and putative TOP motif (green box). The TOP motif are conserved across *Diptera* (blue). (**B**) Sequence logo generated from motif discovery of CAGE derived TSSs of *ais* translation target genes resemble a canonical TOP motif. (**C**) Histogram representing the location of the first 5-mer polypyrimidine sequence from each CAGE based TSS of *ais* translationally regulated genes demonstrates that the TOP motifs occur proximal to the TSS (n=76 targets). (**D**) Schematic of the *WT* and *Mut-TOP-GFP* reporter constructs. (**E-F”**) Images and quantifications of (**E-E’**) *WT-TOP-GFP* and (**F-F’**) *Mut-TOP-GFP* reporter expression stained for 1B1 (red), GFP (green, grayscale), and Vasa (blue). Yellow line marks increased reporter expression in 8-cell cysts of *WT-TOP-GFP* but not in *Mut-TOP-GFP*. Reporter expression was quantified over germline development for (**E”**) *WT-TOP-GFP* and (**F”**) *Mut-TOP-GFP* and normalized to expression in the GSC. (**G-H’**) Images of *WT-TOP-GFP* reporter ovarioles showing 1B1

(red), GFP (green, grayscale), and Vasa (blue) in (**G-G'**) *bam* GKD and (**H-H'**) *ais* GKD ovaries. Yellow lines denote germline. (**I-J'**) Images of *Mut-TOP-GFP* reporter expression showing 1B1 (red), GFP (green, grayscale), and Vasa (blue) in (**I-I'**) *bam* GKD and (**J-J'**) *ais* GKD. Yellow lines indicate germline. (**K**) Quantification of WT and Mutant TOP reporter expression in undifferentiated daughter cells in *bam* GKD compared *ais* GKD demonstrates that the *WT-TOP-GFP* reporter shows significantly lower expression in *ais* GKD than the *Mut-TOP-GFP* relative to the expression of the respective reporters in *bam* GKD (n=17–25 germaria per genotype, with Welch's t-test ***=$p<0.001$). Scale bars are 15 μm.

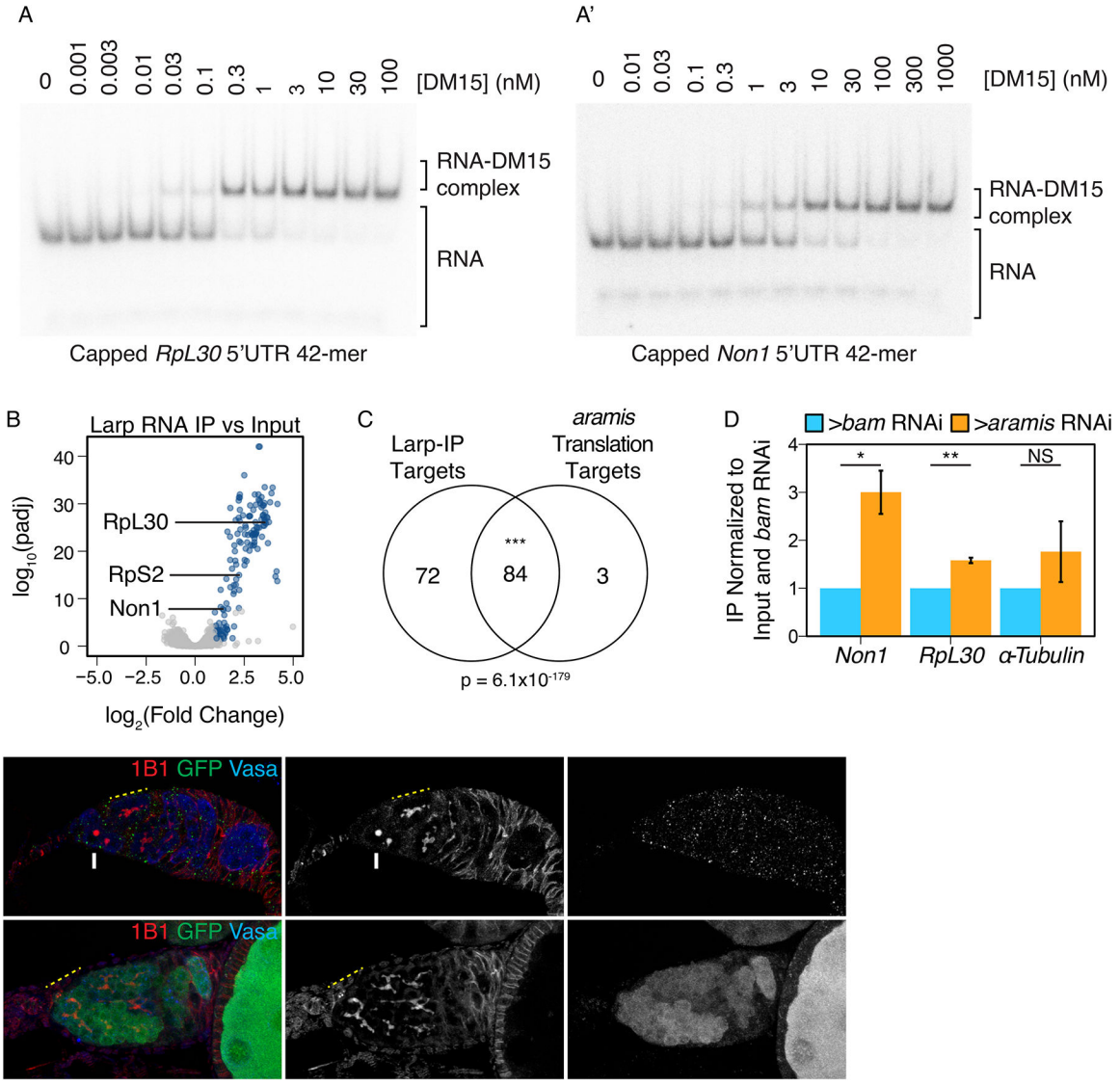


**Figure 7. Larp binds to TOP mRNAs and binding is regulated by Ais.**

(**A-A'**) EMSA of Larp-DM15 and the leading 42 nucleotides of (**A**) *RpL30* and (**A'**) *Non1* indicates that both RNAs bind to Larp-DM15. (**B**) Volcano plot of mRNAs in Larp::GFP::3XFLAG IP vs input showing mRNAs significantly enriched in Larp::GFP::3XFLAG (blue). (**C**) Venn diagram of overlapping Larp IP targets and *ais* GKD polysome-seq targets overlap ($p<0.001$, Hypergeometric Test). (**D**) Bar plot representing the fold enrichment of mRNAs from Larp RNA IP in *ais* GKD relative to control ovaries measured with qPCR (n=3, *=$p<0.5$, **=$p<0.01$, NS = nonsignificant, one-sample t-test, mu=1). Data are mean±SE. (**E-F"**) Images of (**E-E"**) *nosGAL4* control and (**F-F"**) ovaries overexpressing the Larp-DM15 stained for 1B1 (red, left grayscale), Vasa (blue), and Larp-DM15::GFP (green, right grayscale). OE of Larp-DM15 results in an accumulation of cysts (yellow line). Scale bars are 15 μm.

## Key Resources Table

| REAGENT or RESOURCE | SOURCE | IDENTIFIER |
|---|---|---|
| Antibodies | | |
| mouse anti-1B1 | Developmental Studies Hybridoma Bank | Antibody Registry ID: 528070 |
| Rabbit polyclonal anti-Vasa | Rangan Lab | N/A |
| Chicken polyclonal anti-Vasa | Rangan Lab | N/A |
| rabbit anti-pTyr | Sigma Aldrich | T1235 |
| rabbit anti-pMad | Abcam | ab52903 |
| rabbit anti-GFP | Abcam | ab6556 |
| mouse anti-p53 | Developmental Studies Hybridoma Bank | Antibody Registry ID: 579787 |
| Rabbit anti-CycB | Santa Cruz Biotechnology | 25764 |
| Rabbit anti-Fibrillarin | Abcam | ab5821 |
| Mouse anti-Fibrillarin | Fuchs Lab | N/A |
| Anti-rabbit Alexa 488 | Jackson ImmunoResearch Labs | 715-545-151 |
| Anti-mouse Cy3 | Jackson ImmunoResearch Labs | 715-165-150 |
| Anti-rabbit Alexa Cy5 | Jackson ImmunoResearch Labs | 711-175-152 |
| Anti-chicken Alexa Cy5 | Jackson ImmunoResearch Labs | 703-175-155 |
| Anti-mouse Alexa Cy5 | Jackson ImmunoResearch Labs | 715-175-151 |
| Mouse anti-FLAG-HRP | Sigma Aldrich | A8592 |
| Mouse anti-FLAG | Cell Signaling | 14C10 |
| Bacterial and Virus Strains | | |
| XL-10 Gold Ultracompetent cells | Integrated Sciences | #200315 |
| Chemicals, Peptides, and Recombinant Proteins | | |
| Formaldehyde (Methanol Free), 10% Ultrapure | Polysciences Inc. | #04018-1 |
| Donkey Serum | Sigma-Aldrich | D9663 |
| Vectashield Antifade Mounting Medium with DAPI | Vector Laboratories | #H-1200 |
| Triton X-100 detergent | VWR | #97062-208 |
| Nonidet P-40 (NP-40) substitute | IBI Scientific | #9016-45-9 |
| Tween-20 detergent | VWR | #97062-332 |
| TRIzol | Invitrogen | #15596026 |
| Complete, EDTA-free Protease Inhibitor Cocktail Pill | Sigma-Aldrich | 11873580001 |
| HiFi Assembly Master Mix | New England Biolabs Inc | E2621S |
| Restriction Endonuclease NotI | New England Biolabs Inc | R0189S |
| Restriction Endonuclease SpeI-HF | New England Biolabs Inc | R3133S |
| Gateway Clonase II | Invitrogen | #12535-029 |
| Dynabeads Protein G | Invitrogen | 10003D |
| 4X Laemmli Sample Buffer | Bio-Rad | #161-0747 |
| SuperScript II | Invitrogen | 18064022 |

| REAGENT or RESOURCE | SOURCE | IDENTIFIER |
|---|---|---|
| RNaseOUT™ Recombinant Ribonuclease Inhibitor | Invitrogen | 10777019 |
| Shields and Sang powdered medium | Sigma-Aldrich | S8398 |
| Yeast Extract | Sigma | Y-1000 |
| Bactopeptone | Difco | 211677 |
| Schneider's media | Gibco | 21720024 |
| proteinase K | NEB | P8107S |
| Critical Commercial Assays | | |
| TURBO DNA-free Kit | Life Technologies | AM1907 |
| SYBR Green Master Mix | Applied Biosystems | #4367659 |
| NEXTFLEX® Rapid Directional RNAseq Library Prep Kit | Bioo Scientific Corp. | NOVA-5138-08 |
| Click-iT™ Plus OPP Alexa Fluor™ 488 Protein Synthesis Assay Kit | Invitrogen | C10456 |
| Mini-PROTEAN TGX 4-20% gradient SDS-PAGE gels | Bio-Rad | #456-1094 |
| Pierce™ ECL Western Blotting Substrate | Thermo Scientific™ | 32106 |
| SuperSignal™ West Pico PLUS Chemiluminescent Substrate | Thermo Scientific™ | 34579 |
| Deposited Data | | |
| RNAseq Data | This study | GSE171350 |
| CAGE-seq Data | (Boley et al., 2014) | SRR488282 |
| Experimental Models: Cell Lines | | |
| DRSC-S2 cells | Drosophila Genomics Resource Center | Stock #181 |
| Experimental Models: Organisms/Strains | | |
| *UAS-Dcr2;nosGAL4* | Bloomington Drosophila Stock Center | 25751 |
| *nosGAL4;MKRS/TM6* | Bloomington Drosophila Stock Center | 4442 |
| Ais RNAi#1 CG5589$^{HMS00325}$ | Bloomington Drosophila Stock Center | 32334 |
| Ath RNAi#1 CG4901$^{HMC04417}$ | Bloomington Drosophila Stock Center | 56977 |
| Pths RNAi#1 CG9253$^{GL00549}$ | Bloomington Drosophila Stock Center | 36589 |
| UAS-tkv.CA | Bloomington Drosophila Stock Center | 36537 |
| bam RNAi$^{HMS00029}$, | Bloomington Drosophila Stock Center | 33631 |
| p53$^{5A-1-4}$ | Bloomington Drosophila Stock Center | 6815 |
| Harwich | Bloomington Drosophila Stock Center | 4264 |
| p53$^{11-1B-1}$ | Bloomington Drosophila Stock Center | 6816 |
| FUCCI: UASp-GFP. E2f1.1-230, UASp-mRFP1.CycB.1-266/TM6B | Bloomington Drosophila Stock Center | 55101 |
| UAS-EGFP | Bloomington Drosophila Stock Center | 5431 |
| ais$^{f06152}$ Pbac{WH}CG5589f06152/TM6B, Tb1 | Bloomington Drosophila Stock Center | 18942 |
| ath Df Df(2L)BSC143/CyO | Bloomington Drosophila Stock Center | 9503 |
| pths$^{KG}$ P{SUPor-P}CG9253$^{KG05120}$ | Bloomington Drosophila Stock Center | 13988 |
| bam RNAi P{TriP.HMJ22155} | Bloomington Drosophila Stock Center | 58178 |
| Non1 RNAi P{TriP.HMS05872} | Bloomington Drosophila Stock Center | 78777 |

| REAGENT or RESOURCE | SOURCE | IDENTIFIER |
|---|---|---|
| Larp::GFP::3XFLAG Mi{PT-GFSTF.1}larp$^{MI06928\text{-}GFSTF1}$ | Bloomington Drosophila Stock Center | 61790 |
| w[1118]; Df(3R)Hsp70A, Df(3R)Hsp70B | Bloomington Drosophila Stock Center | 8841 |
| Nprl3 RNAi P{TriP.HMC04072}attP40 | Bloomington Drosophila Stock Center | 55384 |
| raptor RNAi P{TriP.HMS00124}attP2 | Bloomington Drosophila Stock Center | 34814 |
| Ais RNAi#2 CG5589$^{v44322}$ | Vienna Drosophila Resource Center | v44322 |
| Ath RNAi#2 CG4901$^{v34905}$ | Vienna Drosophila Resource Center | v34905 |
| Ais::GFP Pbac{fTRG01033.sfGFP-TVPTBF}VK00002 | Vienna Drosophila Resource Center | v318731 |
| Ath::GFP Pbac{fTRG01233.sfGFP-TVPTBF}VK00033 | Vienna Drosophila Resource Center | v318731 |
| Non1::GFP Pbac{fTRG00617.sfGFP-TVPTBF}VK00033 | Vienna Drosophila Resource Center | v318895 |
| UASp-CycB::GFP | Huynh lab | |
| *UAS-Dcr2;nosGAL4;bamGFP* | Lehmann lab | |
| *If/CyO;nosGAL4* | Lehmann lab | |
| w1118 | Lehmann lab | |
| *tjGAL4/CyO* | Lehmann lab | |
| UASp-p53 | Bakhrat lab | |
| RpS2::GFP$^{CB02294}$ | Buszczak lab | |
| UASt-pths::3XFLAG:: 3XHA | Siekhaus lab | |
| UASp-Non1 | This study | |
| UASp-Larp-DM15 | This study | |
| WT-TOP-Reporter | This study | |
| Mutant-TOP-Reporter | This study | |
| Oligonucleotides | | |
| Primers and G-blocks | Supplemental Table 8 | N/A |
| Recombinant DNA | | |
| Plasmid: pCaSpeR2 P element transformation vector | Drosophila Genomics Resource Center | Stock Number: 1066 |
| Gateway Destination Vector Plasmid: pPWG | Drosophila Genomics Resource Center | Gateway 1 Collection |
| Gateway Destination Vector Plasmid: pPGW | Drosophila Genomics Resource Center | Gateway 1 Collection |
| Gateway pDONR 221 Vector | Invitrogen | #12536-017 |
| Software and Algorithms | | |
| ImageJ | Schindelin, J., et al 2012 | https://imagej.nih.gov/ij/ |
| HISAT2 | D. Kim., et al 2015 | https://ccb.jhu.edu/software/hisat2/index.shtml |
| DESeq2 | M.I. Love, et al 2014 | http://www.bioconductor.or2/packa2es/release/bioc/html/DESea2.html |
| featureCounts | Y. Liao, et al 2014 | http://bioinf.wehi.edu.au/featureCounts/ |
| MEME | T.L. Bailey, et al 2006 | https://meme-suite.org/doc/overview.html |
| Homer | Heinz S., et al 2010 | http://homer.ucsd.edu/homer/ |

| REAGENT or RESOURCE | SOURCE | IDENTIFIER |
|---|---|---|
| Biostrings | Pagès H., et al 2021 | https://bioconductor.org/packages/release/bioc/html/Biostrings.html |
| ggplot2 | Wickham H. 2016 | https://cran.r-project.org/web/packages/ggplot2/index.html |
| scales | Wickham H., et al 2020 | https://cran.r-project.org/web/packages/scales/index.html |
| egg | Auguie B. 2019 | https://cran.r-project.org/web/packages/egg/index.html |
| rtracklayer | Lawrence M. et al, 2009 | https://bioconductor.org/packages/release/bioc/html/rtracklayer.html |
| gggenes | Wilkins D. 2020 | https://cran.r-project.org/web/packages/gggenes/index.html |
| FastQC | Andrews, S. (2010) | https://www.bioinformatics.babraham.ac.uk/projects/fastqc/ |